TOPICAL REVIEW • OPEN ACCESS

Dielectric optical nanoantennas

To cite this article: Md Rabiul Hasan and Olav Gaute Hellesø 2021 *Nanotechnology* **32** 202001

View the article online for updates and enhancements.

Topical Review

Dielectric optical nanoantennas

Md Rabiul Hasan and Olav Gaute Hellesø

Department of Physics and Technology, UiT—The Arctic University of Norway, Tromsø, Norway

E-mail: olav.gaute.helleso@uit.no

Abstract

Nanophotonics allows the manipulation of light on the subwavelength scale. Optical nanoantennas are nanoscale elements that enable increased resolution in bioimaging, novel photon sources, solar cells with higher absorption, and the detection of fluorescence from a single molecule. While plasmonic nanoantennas have been extensively explored in the literature, dielectric nanoantennas have several advantages over their plasmonic counterparts, including low dissipative losses and near-field enhancement of both electric and magnetic fields. Nanoantennas increase the optical density of states, which increase the rate of spontaneous emission due to the Purcell effect. The increase is quantified by the Purcell factor, which depends on the mode volume and the quality factor. It is one of the main performance parameters for nanoantennas. One particularly interesting feature of dielectric nanoantennas is the possibility of integrating them into optical resonators with a high quality-factor, further improving the performance of the nanoantennas and giving very high Purcell factors. This review introduces the properties and parameters of dielectric optical nanoantennas, and gives a classification of the nanoantennas based on the number and shape of the nanoantenna elements. An overview of recent progress in the field is provided, and a simulation is included as an example. The simulated nanoantenna, a dimer consisting of two silicon nanospheres separated by a gap, is shown to have a very small mode volume, but a low quality-factor. Some recent works on photonic crystal resonators are reviewed, including one that includes a nanoantenna in the bowtie unit-cell. This results in an enormous increase in the calculated Purcell factor, from 200 for the example dimer, to 8×10^6 for the photonic crystal resonator. Some applications of dielectric nanoantennas are described. With current progress in the field, it is expected that the number of applications will grow and that nanoantennas will be incorporated into new commercial products. A list of relevant materials with high refractive indexes and low losses is presented and discussed. Finally, prospects and major challenges for dielectric nanoantennas are addressed.

Keywords: nanophotonics, dielectric materials, nanoantennas

(Some figures may appear in colour only in the online journal)

1. Introduction

Antennas for radio and microwave wavelengths are widely used as an integral part of wireless communications. Compared to conventional antennas, optical nanoantennas are less common, mainly due to their small size. Advances in nanoscience and fabrication technologies have made it possible to realize structures down to nanometers [1], thus paving the way for new and improved designs of optical nanoantennas. The emergence of optical nanoantennas has opened new research directions and applications. Among the diverse applications are nanoparticle trapping [2–4], optical sensing [5–8], optical computing [9–12], and spectroscopy [13–17].
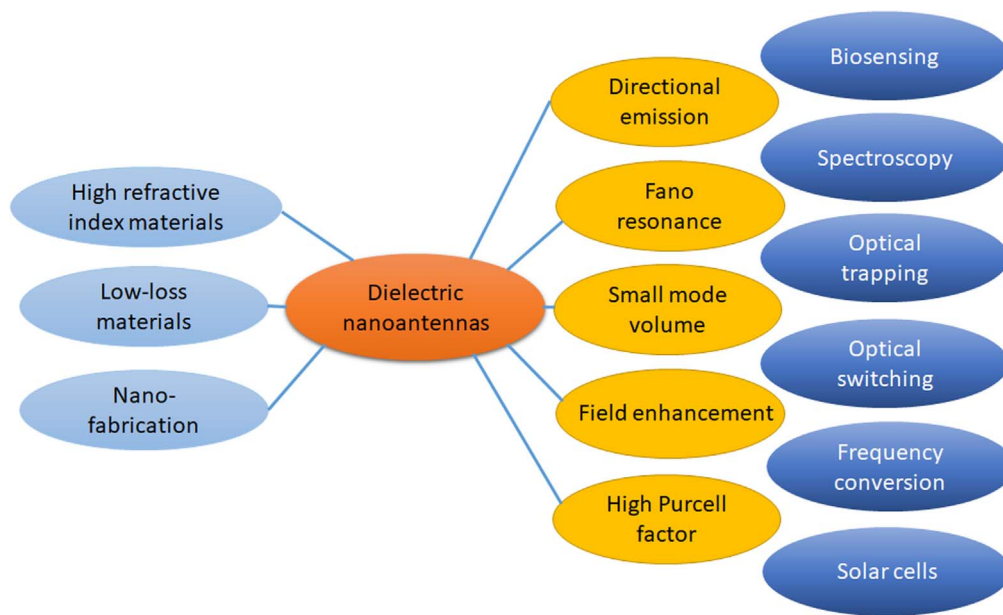
Figure 1. Schematic illustration of the factors necessary to realize dielectric optical nanoantennas, their main optical properties, and some applications.

Figure 1 illustrates the factors necessary to realize dielectric optical nanoantennas, their optical properties and some applications.

Optical nanoantennas can be categorized into three types: (a) plasmonic or metallic nanoantennas, (b) metal-dielectric nanoantennas, and (c) dielectric nanoantennas. Different configurations of plasmonic and metal-dielectric nanoantennas have been investigated and reviewed [18–27]. They include monopole nanoantennas, dimer nanoantennas, dipole nanoantennas, bowtie nanoantennas, core–shell nanospheres, Yagi-Uda nanoantennas, nanoflower arrays, directed scatterers, rhombic nanoantennas, and hybrid nanoantennas. Several metal-dielectric nanoantennas with active coatings have also been reported for enhanced scattering [27–30]. Active coatings have practical limitations, as the scattering becomes dependent on shape and polarization [27]. Plasmonic nanoantennas have two major drawbacks. First, they exhibit high optical loss due to the interband transitions of most commonly used plasmonic metals such as gold and silver [31, 32]. Therefore, they suffer from low antenna radiation efficiency. Second, the dissipative losses in metals generate heat in the nanoantenna structures and the surrounding environment [31, 32]. This is detrimental for several applications such as for heat-sensitive biological samples and optical trapping of nanoparticles, which are propelled out of the trap by thermally induced flows. In contrast, dielectric nanoantennas show considerably lower absorption loss and insignificant Joule heating, compared to their plasmonic counterparts. Therefore, they pave the way for new biological applications where negligible local heating is essential. Dielectric materials with a high refractive index offer enhancement of both electric and magnetic fields [33], which can be used to control the scattered radiation.

Dielectric optical nanoantennas can provide exceptionally small mode volumes, as demonstrated in several works that will be reviewed. The review also includes the simulation of a dimer consisting of two silicon nanospheres separated by a small gap. This can be considered a basic example of an optical nanoantenna. The simulation shows that a very small gap also gives a very small mode volume. A notable advantage of dielectric nanoantennas is the possibility of integration with optical resonators. Optical resonators give added enhancement of the field by accumulating light on many roundtrips, and due to their low losses, nanoantennas can potentially be integrated in the resonator without reducing its quality factor. Such a combination can be realized by incorporating a nanoantenna in a photonic crystal resonator. Recent work and the state-of-the-art in this direction will be discussed and compared with the example dimer nanoantenna.

The fabrication technologies for dielectric materials are mature and allow us to realize compact, low-cost and integrated nanophotonic devices [1]. Over the last decade, several dielectric nanoantenna structures have been reported including microspheres [34–36], nanospheres [37–40], Yagi-Uda nanoantennas [41–45], core–shell nanoantennas [46–48], dimers [31, 32, 49–56], bowtie nanoantennas [57–59], nanodisks [60–62] and nanorods [63, 64]. The objective of this review is to (i) define the terminology and performance parameters, (ii) give an overview of recent progress in the field and compare some of the results, (iii) describe some potential applications, (iv) list and discuss suitable materials, and (v) discuss the future outlook and challenges for dielectric optical nanoantennas.

2. Definitions and performance parameters

In classical antenna theory, antennas are devices that transform alternating currents (electric and magnetic) to
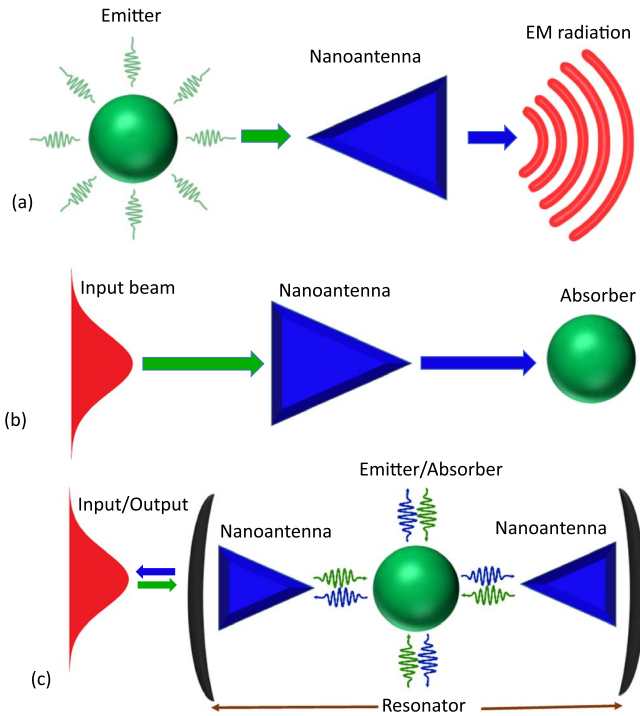
Figure 2. Outline of (a) a transmitting nanoantenna, (b) a receiving nanoantenna, and (c) a transmitting or receiving nanoantenna integrated in an optical resonator.

electromagnetic (EM) waves or EM waves to alternating currents. This definition is somewhat vague and inappropriate when it comes to defining optical nanoantennas. In general, optical nanoantennas serve as transducers between free EM radiation and localized energy [65]. Whereas an optical lens can focus a beam to a diffraction-limited spot, optical nanoantennas work with the near-field and, as a consequence, do not have a diffraction limit *per se*.

The interactions of a nanoantenna with an emitter or an absorber are illustrated in figures 2(a), (b). The emitter is taken as a point source that radiates isotropically, e.g. a fluorescent nanoparticle. Another example of an emitter can be an oscillating electric or magnetic dipole. The role of the transmitting nanoantenna is to enhance and pick up the emitted, highly diverging field, and transform it into a field that can be captured by a detector, e.g. a microscope. Similarly, a receiving nanoantenna transforms an incident field, e.g. a plane wave or a Gaussian beam, into a highly localized field, which is captured by an absorber [65]. As for the emitter, the absorber is much smaller than the operating wavelength. In principle, the two cases of transmitting and receiving nanoantennas are reversible and their respective output and input field-distributions can be of any shape depending on the application. However, as a detector only sees the amplitude of the field, the output field-distribution from a transmitting nanoantenna is often less critical than the input field for the receiving nanoantenna. To obtain high localized intensity on an absorber, a laser and thus a Gaussian field-distribution is most common. This is thus taken as the input beam for the absorber in figure 2(b). Alternatively, for simultaneous excitation of many receiving nanoantennas, a wide beam or a plane wave can be used, which is the case for solar cells. A dielectric nanoantenna can be embedded inside an optical resonator in both transmitting and receiving modes as shown in figure 2(c). In transmitting mode, radiation from the emitter is captured by the nanoantenna and enhanced by the resonator, which produces an output beam. Reversely, in the receiving mode, the resonator builds up a strong field, which the nanoantenna transforms to a localized field, which in turn is captured by the absorber. In both cases, the resonator builds up the field over many cycles and enhances the energy density in the confined field, thus increasing the performance of the nanoantenna.

Optical nanoantennas resemble their classical counterparts. However, several important differences exist in terms of scaling and physical characteristics. In the following section, we will describe the most important performance parameters for nanoantennas, without giving a full theoretical treatment. Interested readers can follow [66, 67] for more extensive theory and definition of other parameters of dielectric nanoantennas.

2.1. Antenna efficiency and directivity

A nanoantenna experiences dissipative losses mostly by heat and absorption, which are low for dielectric materials, but must be accounted for. Antenna efficiency or radiation efficiency measures the degree of these losses. It is defined as the ratio of far-field radiated power to total power dissipated by the nanoantenna. Mathematically, the radiation efficiency of a nanoantenna is expressed by [68],

$$\varepsilon_{\mathrm{rad}} = \frac{P_{\mathrm{rad}}}{P} = \frac{P_{\mathrm{rad}}}{P_{\mathrm{rad}} + P_{\mathrm{loss}}}, \qquad (1)$$

where P accounts for the total power dissipated by the nanoantenna, which consists of radiated power P_{rad} and total power loss P_{loss} of the nanoantenna. For a lossless hypothetical nanoantenna, the radiation efficiency is unity.

The directivity (D) of a nanoantenna measures the ability to concentrate radiated power in a particular direction. It is a comparative measure for how much the radiated power is enhanced if an isotropic antenna (an antenna that radiates power in all directions equally) is replaced by a directional antenna. In general, a narrow radiation pattern provides high directivity. The general expression for directivity is given by,

$$D(\theta, \phi) = \frac{4\pi}{P_{\mathrm{rad}}} p(\theta, \phi), \qquad (2)$$

where the angles θ and ϕ are measured in the spherical coordinate system and indicate the direction of observation. The normalized angular power density $p(\theta, \phi)$ defines the angular distribution of the radiated power, which is related to P_{rad} by the following expression,

$$P_{\mathrm{rad}} = \int_0^\pi \int_0^{2\pi} p(\theta, \phi) \sin\theta \, \mathrm{d}\phi \, \mathrm{d}\theta \qquad (3)$$

When the direction (θ, ϕ) is not clearly stated, the direction of maximum directivity (D_{max}) is often used. Mathematically,

$D_{\max}$ is given by $D_{\max} = \frac{4\pi \, Max[p(\theta, \phi)]}{P_{\mathrm{rad}}}$, where $\mathrm{Max}[p(\theta, \phi)]$ is the radiation power transmitted by the main lobe.

2.2. Cross sections and field enhancement factors

Let us assume a spherical, dielectric nanoparticle with radius r and illuminated by a plane wave having intensity I_0. Some of the power from the plane wave will be captured by the particle and concentrated in its near-field. The nanoparticle thus acts as a nanoantenna. A small fraction of the plane wave will be absorbed and scattered by the particle, and the plane wave will thus experience a small attenuation. For a plane wave, the intensity $I_0 = n_s |E_{\mathrm{in}}|^2 / 2Z_0$, where n_s is the refractive index of the surrounding medium, E_{in} is the amplitude of the incident electric field and Z_0 is the impedance of free space. The net rate of EM energy passing across the surface of the nanoparticle is given by $\mathbf{S} \cdot \hat{\mathbf{e}}A$, where $\mathbf{S}$ is the Poynting vector, and A is the area defined by the unit normal vector $\hat{\mathbf{e}}$. The scattering cross section is found by,

$$C_{\mathrm{scat}} = \frac{1}{I_0} \iint (\mathbf{S}_S \cdot \hat{\mathbf{e}}) \mathrm{d}A, \tag{4}$$

where $\mathbf{S}_s$ is the Poynting vector for the scattered radiation. The integration is performed over the closed surface of the nanoparticle.

The absorption cross section is given by the following expression,

$$C_{\mathrm{abs}} = \frac{1}{I_0} \iiint P_{\mathrm{d}} \, \mathrm{d}V, \tag{5}$$

where P_{d} is the power loss density in the nanoparticle and the integration must be performed over its volume V.

The extinction cross section, which is a measure of the attenuation experienced by the plane wave, is the sum of the scattering and absorption cross sections:

$$C_{\mathrm{ext}} = C_{\mathrm{abs}} + C_{\mathrm{scat}} \tag{6}$$

The virtual scattering cross section of the nanoparticle is different from the physical scattering cross section. Three dimensionless parameters called efficiency factors, are used to relate the virtual and the physical scattering cross section. The efficiency factors for absorption, scattering and extinction are defined by

$$Q_{\mathrm{abs}} = \frac{C_{\mathrm{abs}}}{G}, \;\; Q_{\mathrm{scat}} = \frac{C_{\mathrm{scat}}}{G}, \;\; \text{and} \;\; Q_{\mathrm{ext}} = \frac{C_{\mathrm{ext}}}{G}, \tag{7}$$

where G is the physical cross sectional area of the nanoparticle ($G = \pi r^2$ for a nanosphere). If the incident beam is totally absorbed or scattered by the nanoparticle, the efficiency factors for absorption and scattering cross-sections will be unity. However, some nanoparticles can absorb or scatter more light than what is given by the cross sectional area. Thus, the efficiency factors can be greater than unity.

The concentration of electric and magnetic fields by nanoantennas is measured by field enhancement factors. The electric field enhancement factor δ^e is defined as the ratio of absolute electric field strength $|\mathbf{E}|$ at a given location in the presence of a nanoantenna, to the absolute electric field strength $|\mathbf{E}_0|$ in the absence of a nanoantenna. Depending on the value of $|\mathbf{E}|$ and $|\mathbf{E}_0|$, the electric field enhancement factor can be either greater or less than unity. Likewise, we can define the magnetic field enhancement factor δ^m, where electric fields $|\mathbf{E}|$ and $|\mathbf{E}_0|$ are replaced by magnetic fields $|\mathbf{H}|$ and $|\mathbf{H}_0|$, respectively.

2.3. Quality factor and mode volume

When a nanoantenna is placed inside an optical resonator, it produces an enhanced light–matter interaction. Moreover, dielectric nanoparticles with high refractive index behave as resonators on their own. The performance of such nanoantennas is characterized by two figures of merit: quality-factor and mode volume. The quality factor Q is a measure of photon cavity lifetime. The quality factor of an optical cavity mode can be defined by the following expression,

$$Q = 2\pi \nu_0 \left(\frac{E_{\mathrm{stored}}}{P_{\mathrm{loss}}} \right) \tag{8}$$

where ν_0 denotes the resonance frequency, E_{stored} is the stored EM energy in the cavity and P_{loss} is the power loss per cycle. Once the resonance profile is obtained, the quality factor can be determined from the resonance peak by fitting it to a Lorentzian lineshape function. In this case, the quality factor can be calculated from $Q = \nu_0 / \Delta\nu$, where $\Delta\nu$ refers to the full-width-at-half-maximum (FWHM) of the resonance peak. The cavity modes have a finite lifetime due to the dissipation of energy in the cavity. The lifetime is expressed by $1/\gamma_{\mathrm{cav}} = 2\mathrm{Im}[\omega_N]$, where γ_{cav} is the cavity decay rate and $\mathrm{Im}[\omega_N]$ is the imaginary part of the complex resonance frequency. The cavity decay rate is related to the quality factor by $Q = \omega / 2\gamma_{\mathrm{cav}}$. In practice, the cavity decay rate has contributions from both radiative and absorption components as given by $\gamma_{\mathrm{cav}} = \gamma_{\mathrm{cav}}^{\mathrm{rad}} + \gamma_{\mathrm{cav}}^{\mathrm{loss}}$. The quality factor is then found from $Q^{-1} = Q_{\mathrm{rad}}^{-1} + Q_{\mathrm{loss}}^{-1}$, where Q_{rad}^{-1} is the decay rate due to radiation to air (or surrounding medium) and Q_{loss}^{-1} is the rate of loss due to absorption.

The mode volume V_m is a measure of the spatial spread and energy density of an optical mode. It represents the ability of a nanoantenna to concentrate the field into a tightly confined spot. For low losses, mode volume is given by [69],

$$V_m = \frac{\int \varepsilon(r) |E(r)|^2 \mathrm{d}V}{\mathrm{Max}(\varepsilon(r) |E(r)|^2)} \tag{9}$$

where E is the electric field and ε is the dielectric constant, which are both spatially dependent. In some cases, the mode volume can be significantly smaller than the physical volume of the nanocavity. For plasmonic nanostructures, a mode volume in the order of $10^{-3} \, (\lambda/n)^3$ has been reported [70]. Here, n is the refractive index of the surrounding material or in the nanocavity. Dielectric nanoantennas have been proposed with similar mode volumes, e.g. $5 \times 10^{-4} \, (\lambda/n)^3$ [71].
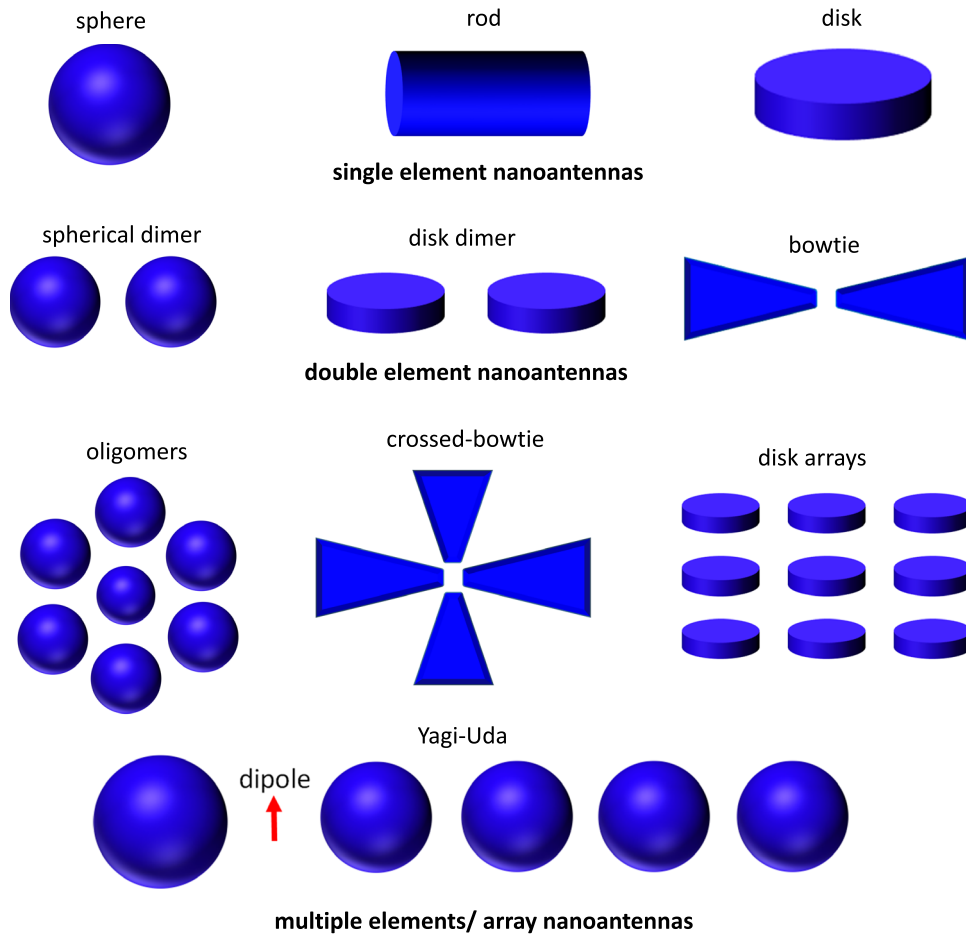
Figure 3. Classification of dielectric optical nanoantennas and illustration of their shapes.

The expression for mode volume must be modified if the nanocavity exhibits high dissipative rates, for which a complex mode volume is used.

2.4. Purcell effect and Purcell factor

As noted, when defining the various parameters, transmitting and receiving nanoantennas can enhance the efficiency of a quantum emitter and detector. The enhancement mechanism can be explained by the Purcell effect. Here, we will consider the Purcell effect for a nanoantenna in transmitting mode. It increases the efficiency of a quantum emitter, which has a finite number of discrete and stationary energy states [72]. When the emitter is excited, it should ideally stay in one of the energy states endlessly. However, the lifetime of the emitter's excited states is reduced because of interaction with the surrounding environment. Such interactions cause an emission of photons by spontaneous transition of the excited emitter into a lower energy state. Previously, it was thought that this spontaneous radiation occurs due to intrinsic characteristics of the atoms. This notion was proved wrong by the pioneering work of E. M. Purcell [73], who showed that the spontaneous relaxation rate of a magnetic dipole can be enhanced compared to the relaxation rate in free space, thus modifying the emission characteristics of the emitter. This phenomenon has been coined the Purcell effect. Based on this effect, the spontaneous emission rate γ_{mol} can be increased using nanoantennas, and the increase is described by the Purcell factor F_p,

$$F_p = \frac{\gamma_{mol}}{\gamma_{mol}^0} = \frac{2g^2}{\gamma_{cav}\gamma_{mol}^0} \qquad (10)$$

where $\gamma_{mol} = 2g^2/\gamma_{cav}$ is the spontaneous emission rate of the emitter in the presence of a nanoantenna, g is the coupling constant, γ_{cav} is the cavity decay rate, $\gamma_{mol}^0 = \frac{nd^2\omega^3}{3\pi\hbar\varepsilon_0 c^3}$ is the decay rate into free space without the nanoantenna, d is the dipole moment, and $\hbar$ is the reduced Planck constant. Equation (10) demonstrates that γ_{mol} of an emitter can be modified by the interplay with a nanocavity. The modification can be large when the resonant frequency of the nanocavity is tuned to the emission frequency of the emitter. Altering the emission lifetime of a quantum emitter with a nanoantenna has potential applications in spectroscopy and optical sensing.

The Purcell factor is related to the quality-factor and mode volume of the nanocavity by the following expression [74],

$$F_p = \frac{3}{4\pi^2}\left(\frac{\lambda}{n}\right)^3\frac{Q}{V_m}. \qquad (11)$$

Equation (11) indicates that the Purcell factor is directly proportional to the quality factor of the cavity and inversely
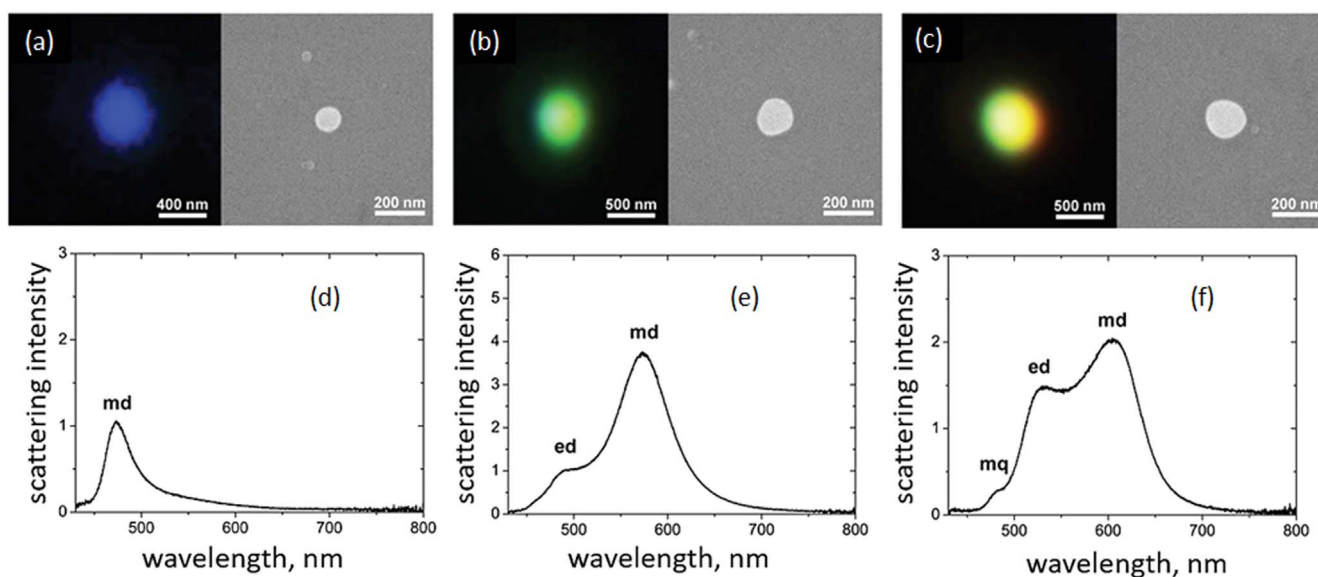
Figure 4. Illustration of Mie resonances in spherical Si nanoparticles. Dark-field microscope image (top left) and scanning electron microscope (SEM) image (top right) of spherical Si nanoparticles with (a) diameter $d = 100$ nm, (b) $d = 140$ nm, and (c) $d = 180$ nm, respectively. (d)–(f) Dark-field scattering spectra for (a), (b) and (c), respectively. Reproduced with permission from [107], © 2012, Nature Publishing Group.

proportional to the mode volume. To obtain a high Purcell factor, it is thus necessary to use a resonator with high quality factor and a nanocavity with a small mode volume.

The Purcell factor quantifies the enhancement of spontaneous emission for a perfect dipole [75]. The Purcell effect contributes to the enhancement of fluorescence and Raman scattering. These effects have been demonstrated for nanoantennas, as will be reported in the next section. For a discussion of the relationship between (theoretical) Purcell factor and (measured) fluorescence enhancement and Raman gain, see [76, 77].

3. Types of dielectric nanoantennas and their optical properties

High refractive index materials (e.g. silicon and germanium) have been used to make optical nanoantennas. These nanoantennas can have different shapes, including spheres [37–40], cylinders/disks [51, 78] and rods [63, 64]. Dielectric nanoantennas can be loosely grouped in three categories based on the number of nanoantenna elements: (i) single element nanoantennas, (ii) double element nanoantennas, and (iii) multiple elements or nanoantenna arrays. Single element nanoantennas include single nanospheres (monomers) [37–40, 79], single nanorods [63, 64] and single nanodisks [80–82]. Double element nanoantennas can consist of two dielectric nanoparticles or nanospheres (dimers) [55, 56, 83–88], two cylindrical nanodisks (nanodisk dimers) [51, 83, 89–93] or two tips as for bowtie nanoantennas [69, 71]. Multiple element or array nanoantennas are taken as any larger group of elements, such as two crossed-bowtie nanoantennas [57], Yagi-Uda nanoantennas [42, 45, 94], oligomers [95–99], and nanodisks arrays [100–102]. Figure 3

illustrates this classification of dielectric nanoantennas with their element types and schematic diagrams.

3.1. Scattering characteristics and resonances for single nanoparticles

Dielectric spherical nanoparticles with a characteristic dimension of a few hundred nanometers show unique scattering characteristics, as will be described in this section. The scattering characteristics are closely linked to the resonances of the particles. The resonances of spheres can be analytically predicted using Mie theory if the refractive index n and size parameter $q = \pi D/\lambda$ are specified [103], where D is the diameter and λ is the wavelength. Plasmonic nanoparticles usually show only electric-type resonances. Due to the absence of an EM field inside metallic nanoparticles, they do not show a magnetic response. However, both electric and magnetic resonances, known as the Mie resonances, can be observed in a dielectric spherical nanoparticle. The magnetic response is due to coupling of the incident light with circular displacement currents generated by the electric field inside the nanoparticle. This happens when the operating wavelength inside the particle becomes comparable to the particle's spatial dimensional $D = \lambda/n$. A dielectric nanosphere shows four dominant resonance modes, associated with magnetic dipole (MD), electric dipole (ED), magnetic quadrupole (MQ) and electric quadrupole (EQ) (for details see [103, 104]). Although higher-order multipoles can be excited, their contribution to scattering efficiency is considerably smaller than the magnetic dipole mode for nanoparticles, as will be shown in the next paragraph.

Theoretical investigations of electric and magnetic resonances for near-infrared (NIR) and visible wavelengths have been conducted for spherical silicon (Si) nanoparticles [105, 106]. It was demonstrated that nanoparticles with radii
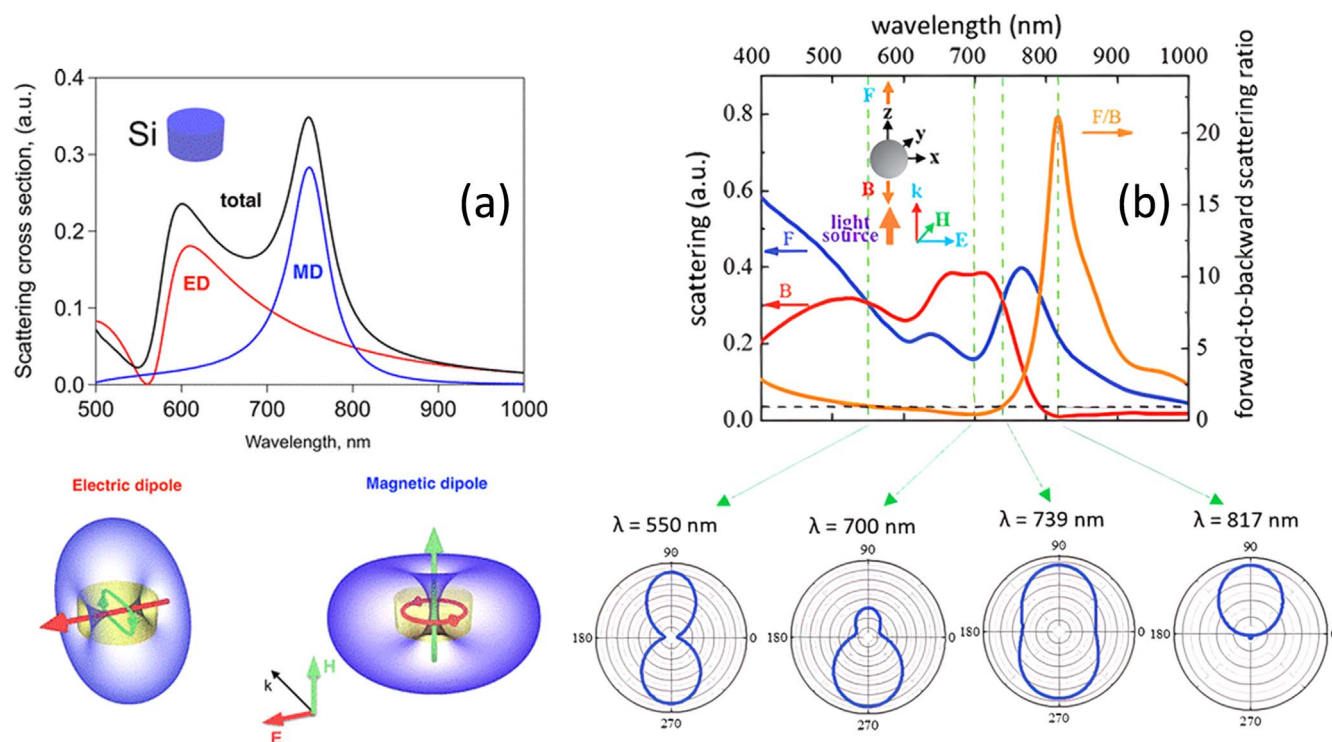
Figure 5. Scattering properties of cylindrical disk and spherical nanoparticles. (a) Numerically calculated scattering contributions for MD and ED resonances of a Si nanodisk with $h = 260$ nm and $d = 400$ nm. Schematic of the radiation patterns are shown in the bottom left. Reproduced with permission from [111], © 2017, ACS. (b) Forward and backward scattering cross-sections, and forward-to-backward scattering ratio of a spherical germanium (Ge) nanoparticle with $d = 150$ nm in free space. Far-field scattering radiation patterns at four different wavelengths are shown in bottom right. Reproduced with permission from [114], © 2017, John Wiley & Sons.

ranging from 65 to 330 nm exhibit electric and magnetic resonances. Experimentally, Mie resonances in spherical Si nanoparticles were reported for visible wavelengths in [107], and as shown in figure 4. Dark-field microscope images, figures 4(a)–(c), show magnetic dipole resonances at different wavelengths for nanoparticle sizes ranging from 100 to 200 nm. For the smallest size, the first resonance appears in the scattering spectra, which corresponds to an MD resonance (figure 4(d)). Increasing the particle size results in a red-shift of the MD resonance, and the appearance of ED (figure 4(e)) and MQ resonances (figure 4(f)). This shows the dominance of the dipole and quadrupole resonances, corresponding to the lower-order Mie resonances, for nanospheres. Mie resonances are not limited to nanospheres, but are also observed for other geometries such as cylindrical disks [108, 109] and rods [64, 110]. Mie resonances in disk-shaped nanoparticles at visible wavelengths have mostly been demonstrated in Si. Figure 5(a) shows electric and magnetic resonances in Si nanodisks with diameter and height of 400 and 260 nm, respectively [111]. As for nanospheres, in addition to the dominant MD and ED resonances, higher-order resonances can exist for larger diameter Si nanodisks, but with minor contributions to the scattering cross sections [80]. Apart from the theoretical investigations, Si nanodisks have been experimentally reported to demonstrate the Mie resonances [82, 108]. Electric and magnetic resonances of nanodisks have also been experimentally studied in other materials. Cylindrical disks of gallium arsenide (GaAs) [112] and

tellurium (Te) [113] were demonstrated at visible and mid-infrared (IR) wavelengths, respectively. Similar to nanospheres and nanodisks, dielectric nanorods can also support electric and magnetic resonances, as shown theoretically in [64] and experimentally in [110] for Si nanorods at visible wavelengths.

The coexistence and coherence of magnetic and electric dipolar resonances inside a dielectric nanoparticle can change the scattering properties and make them dependent on the phase between the magnetic and the electric dipole. Kerker *et al* [115] predicted the conditions necessary to control forward and backward scattering in dielectric particles, known as the Kerker conditions. When the electric and magnetic induced dipoles oscillate at similar magnitude and in-phase, the backward scattering can be made exactly zero (known as the first Kerker or zero backward condition). Correspondingly, near-zero forward scattering can be achieved when the induced dipoles are equal in magnitude but oscillate out-of-phase (the second Kerker or near-zero forward condition). Experimental investigations demonstrated that a dielectric sphere with a diameter of 18 mm and a refractive index of four can mimic the theoretical predictions of Kerker *et al* for microwave wavelengths [116]. Moving to the nano-range, a similar control over scattered radiation has been shown for visible wavelengths with Si nanospheres [117] and with germanium (Ge) nanospheres [114]. For a Ge nanosphere of 150 nm diameter, maximum and minimum forward-to-backward ratios of around 20 and 0.4 were achieved, as shown in
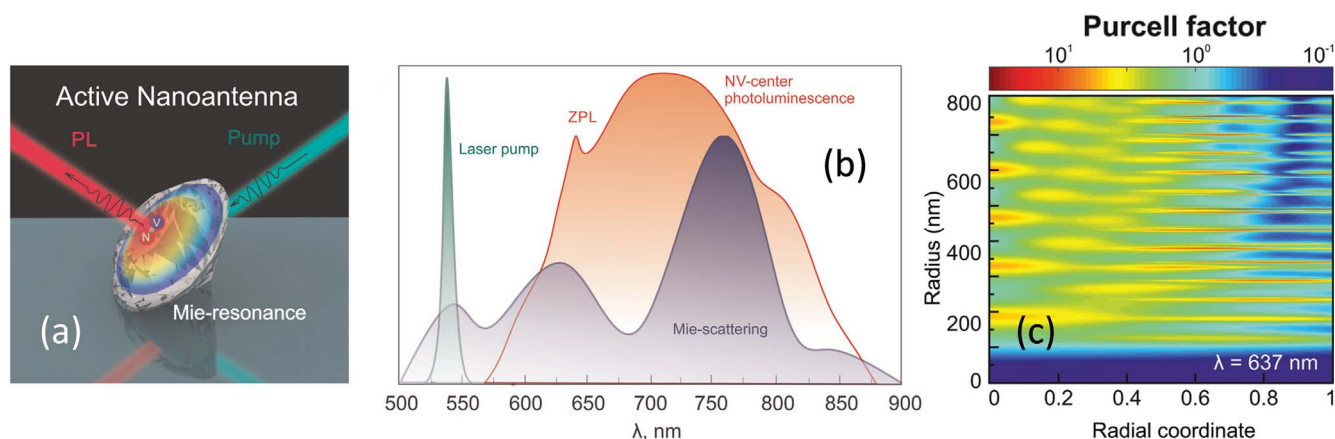
Figure 6. Purcell effect in active diamond nanoantennas. (a) Schematic of a diamond nanosphere with nitrogen vacancy (NV) centers. (b) Spectral overlap of laser pulse, NV-center photoluminescence (PL) spectrum and Mie scattering spectrum of diamond nanosphere. (c) Simulated Purcell factor as a function of radial position of NV-center along the nanosphere radius. Reproduced with permission from [124], © 2018, RSC.

figure 5(b). The scattering radiation patterns show zero backward and near-zero forward scattering at 817 and 700 nm, while an equal forward and backward scattering can be found at 550 and 739 nm, respectively (bottom of figure 5(b)). Similar forward and backward scattering patterns by Ge nanospheres have also been reported in the near-IR region [118]. Going one step further, multilayer nanospheres have been theoretically studied for simultaneously achieving zero backward and nearly-zero forward scattering [119]. As a consequence, the scattering is mainly sideways to the incoming light. Dielectric cylindrical disks can also be used for controlling scattered radiation, as realized in recent reports. Theoretical works demonstrating zero forward scattering can be found in [120, 121], while zero backward scattering was discussed in [112]. Moreover, dielectric nanorods have been investigated recently for achieving zero backward scattering [122]. Dielectric nanospheres can also be used to control the direction of scattering and provide a significant enhancement of directivity compared to the directivity of a point dipole. A Si nanosphere with a notch, and excited by a dipole placed within the notch, can induce higher-order magnetic multipoles, as shown by simulations in [38]. These multipoles contribute to increasing the directivity up to 10 times. Moreover, changing the source dipole position within the notch results in shifting the direction of the radiation, thus enabling a form of beam-steering.

Mie resonances in dielectric nanoparticles can enhance the spontaneous emission rate of an emitter, which is quantified by the Purcell factor (see section 2.4). Theoretically, a Purcell factor of 90 has been shown for a Si nanosphere (diameter 615 nm, NIR-wavelength) for a longitudinal MD excitation, while it was approximately 15 times for a transverse MD excitation [40]. A quantum emitter based on negatively charged nitrogen–vacancy (NV) centers in diamond can be used for the excitation of a Si nanosphere, giving a Purcell factor of up to 50 [123]. Recently, Purcell enhancement in an active diamond nanosphere with NV centers (figure 6(a)) has been studied through simulations and experiments [124]. By tuning the size of the diamond

nanosphere, magnetic and electric resonances can be overlapped with the pump wavelength and the photoluminescence (PL) spectrum of the NV-center (figure 6(b)). This process increases the Purcell factor due to reduction of the emission lifetime, thus enhancing the luminescence emission of NV-centers. The Purcell effect is suppressed for nanospheres with a radius of less than 150 nm and enhanced for larger nanospheres (figure 6(c)). By exciting higher-order Mie resonances in dielectric nanospheres, evanescent fields are produced, which can be utilized for enhancing the Raman signal from organic molecules attached to the nanospheres [37].

3.2. Dimers and field enhancement

The second category of nanoantennas according to figure 3 has two elements in a dimer or bowtie-configuration. A dielectric dimer consists of a pair of spherical or cylindrical nanoparticles and is a widely used configuration for nanoantennas. For dimers, our main focus will be on field enhancement, rather than on the scattering properties considered for single nanoantennas. A single dielectric nanosphere or disk can only provide low near-field enhancement [56]. In a dimer structure, the fields from two nanoparticles can interact in the gap between them, giving a significant enhancement of the near-field. Moreover, by adjusting the dimer gap, a smaller mode volume can be achieved [56, 83] than what is possible with a single nanoparticle. A metallic dimer only generates an electric hotspot when incident light is polarized along the dimer axis, as there is no magnetic hotspot for incident light polarized perpendicular to the dimer axis (figure 7(a)). On the other hand, a dielectric dimer produces both electric and magnetic hotspots in the dimer gap for incident light polarized, respectively, along and perpendicular to the dimer axis (figure 7(b)) [56].

Generation of electric and magnetic hotspots has been demonstrated for both spherical and disk dimers. A Si dimer, consisting of two nanospheres of radius 150 nm and separated by a narrow gap of 4 nm, gives nearly 30 and 13 times
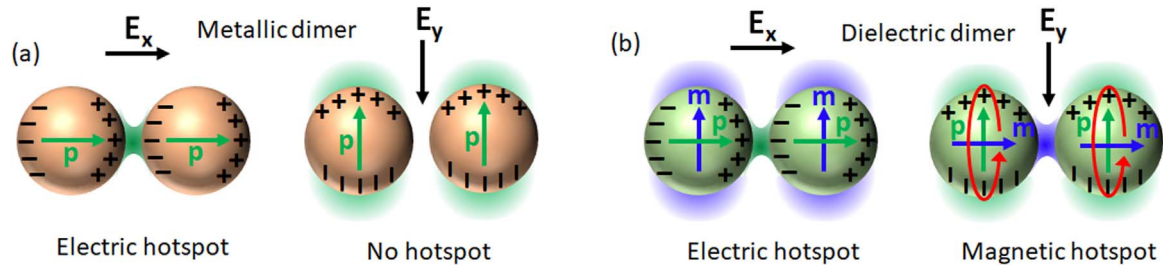
Figure 7. Comparison of hotspots generation in metallic and dielectric dimers. Electric and magnetic hotspots produced in (a) a metallic and (b) a dielectric dimer. The arrows indicate polarization direction of electric field. Here, **p** and **m** indicate electric and magnetic dipole moment. Reproduced with permission from [125] © 2015, ACS.
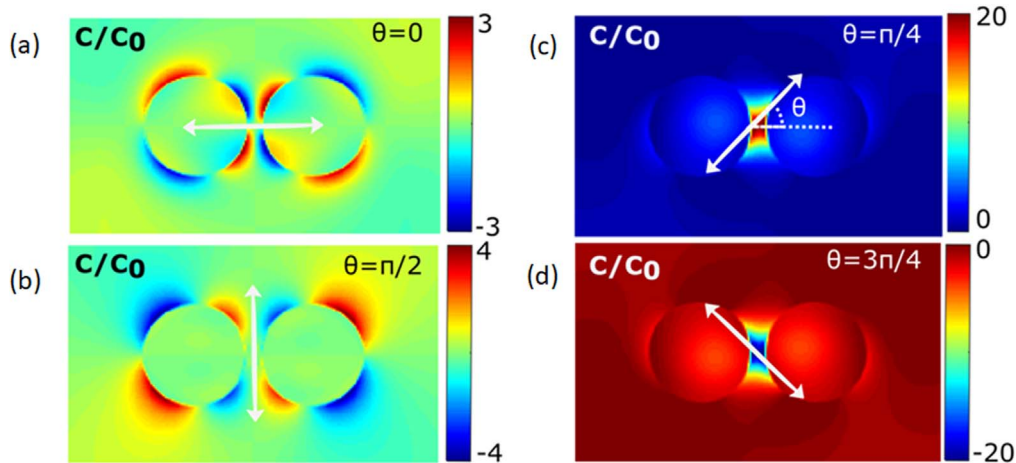
Figure 8. Enhancement of chiral density for a Si dimer for linear polarization relative to chiral density for circular polarization. For polarization (a) parallel and (b) perpendicular to the dimer axis, chiral density (and enhancement of it) is zero in the gap and low elsewhere. For off-axis polarization with (c) incident angle $\theta = \pi/4$ (d) and $3\pi/4$, the enhancement is considerable. Reproduced with permission from [78], © 2019, ACS.

enhancement of electric and magnetic fields in the center of the gap, according to simulations [56]. Field enhancement in hollow spherical Si dimers has also been simulated, showing an enhancement of ten times the magnetic near-field [126]. Electric and magnetic hotspots produced in Si cylindrical dimers were theoretically reported in [91]. Furthermore, the behavior of electric and magnetic resonances in AlGaAs nanopillar dimers has been demonstrated using simulations and cathodoluminescence imaging [127]. It was shown that coupling of adjacent nanopillars occurs due to the splitting of single pillar modes, thus generating symmetric and antisymmetric modes at different wavelengths.

Chirality is a measure of asymmetry. Two molecules are chiral if they are mirror images of each other, and the mirror images cannot be superimposed through translation or rotation. The two chiral molecules are referred to as enantiomers. Enantiomers can have very different chemical properties, making it important to distinguish between them. A difference in absorption for right- and left-handed circularly polarized light can be used to measure the chirality of a sample. A hotspot generated by a nanoantenna can increase the influence of the light–matter interaction on chirality, and thus make it easier to detect and distinguish enantiomers [57, 128, 129]. The influence of the field on chirality is given by the chiral

density of the field, $C = -\frac{\varepsilon_0 \omega}{2} \text{Im}(\boldsymbol{E}^* \cdot \boldsymbol{B})$, where **E** and **B** are the electric and magnetic field vectors, and ω is the angular frequency.

Figure 8 shows a dimer and enhancement of the chirality of the field in the gap, for linear polarization (C) relative to the chiral density for circular polarization (C_0). For polarization along or perpendicular to the axis of the dimer, figures 8(a), (b), the field is not chiral in the gap, due to symmetry. On the other hand, for off-axis polarization, figures 8(c), (d), there is an enhancement of the chirality of up to ± 20 relative to circular polarization [78]. This shows that a dimer can be used for detection of chirality also using linear polarization, and that the sensitivity can be significantly larger than for circular polarization, which is normally used for detecting chirality. In addition to dimers, crossed-bowtie nanoantennas [57] and nanodisks with a slanted slot [130] have been demonstrated numerically for chirality enhancement.

Field enhancement and small mode volume in the dimer gap can increase fluorescence emission and Raman scattering due to the Purcell effect. The fluorescence enhancement in a dimer gap has been measured with fluorescence correlation spectroscopy, indicating that Si dimers provide somewhat higher fluorescence enhancement (around 270-fold) than Au dimers (around 200-fold) for similar configurations (figure 9(b)). Besides, a slightly
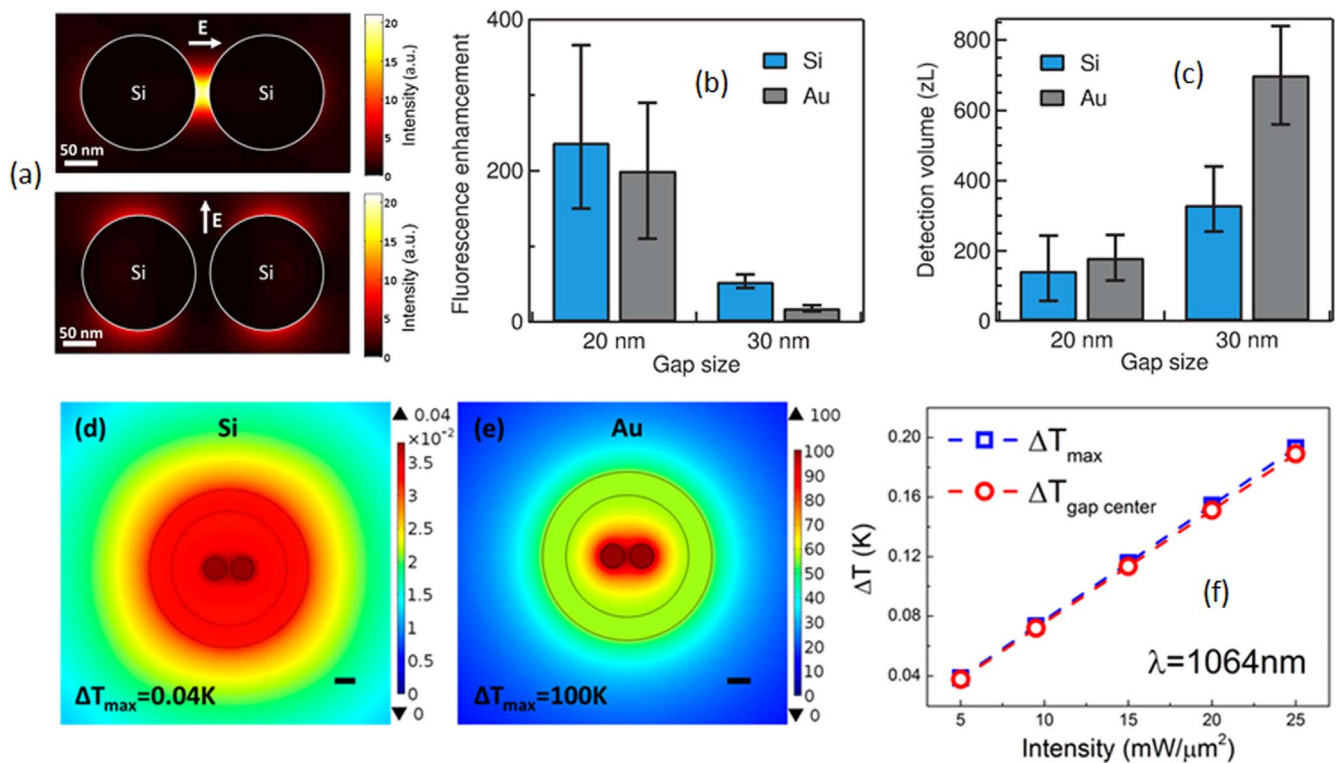
Figure 9. Comparison of fluorescence enhancement, detection volume and temperature rise for Si and Au dimers. (a) Simulated electric field enhancement in the gap of a cylindrical Si dimer with $h = 60$ nm, $g = 20$ nm and $d = 170$ nm. (b) Fluorescence enhancement for Si and Au dimers with gap of 20 and 30 nm. (c) Measured detection volume for Si and Au dimers with gap of 20 and 30 nm. Reproduced with permission from [83], © 2016, ACS. Simulated temperature increase around a (d) Si dimer and an (e) Au dimer with $d = 200$ nm, $h = 200$ nm, $g = 50$ nm and laser intensity of 5 mWμm^{-2}. (f) Simulated temperature increase on the dimer surface (blue square) and in the dimer gap (red circle) for the Si dimer as a function of (trapping) laser intensity. Reproduced with permission from [132], © 2018, ACS.

reduced detection volume was found for the Si dimers for a 20 nm gap, and significantly reduced for a 30 nm gap, as compared to the Au dimers (figure 9(c)). Dielectric dimers enhance Raman scattering by utilizing the field enhancement in the gap. An enhancement of the Raman scattering of $\sim 10^3$ times has been demonstrated in Si dimers [32]. Additionally, surface fluorescence enhancement of ~ 1900 times was found with the same nanoantenna, and up to 3600 times with gallium phosphide (GaP) nanodisks separated by a 35 nm gap [131]. An important aspect of dielectric nanoantennas, and dielectric dimers in particular, is the low heat generation, which enables spectroscopic experiments at constant temperature. Simulation results indicate that the temperature increase around a Si dimer is very small, with a maximum of 0.04 K, while a Au dimer of similar configuration shows a dramatic temperature rise with a maximum of 100 K (figures 9(d), (e)) [32]. Moreover, increasing the laser intensity from 5 to 25 mWμm^{-2} results in a temperature rise from 0.04 to 0.2 K only, (figure 9(f)), thus demonstrating that high laser intensity can be used for nanoparticle trapping (which is the topic of [32]) and with dielectric nanoantennas in general.

The small mode volume and field enhancement of dimers increase the efficiency of quantum emitters and detectors. This increase is typically quantified by the Purcell factor as described in section 2.4. To complete this section, a simulation of a Si dimer is included and its Purcell factor calculated. The dimer, as proposed in [56], consists of two Si nanospheres with a radius 150 nm and separated by a gap. To find

the Purcell factor for the dimer, the quality factor must be known in addition to the mode volume. The finite-element method was used for the 3D simulations (COMSOL v.5.4). For a radius of 150 nm, the dimer shows three resonance peaks in the extinction spectra, which correspond to MD, ED and MQ resonances (see [56]). In the following, only the MD resonance is considered because it has the highest extinction efficiency and the sharpest resonance. The mode volume is calculated in air (i.e., in the dimer gap) using equation (9), and the quality factor is found from the extinction spectra as discussed in sections 2.2 and 2.3. The quality factor and mode volume as a function of the gap is shown in figure 10(a)) for a plane wave with the electric field along the axis of the dimer. Enlarging the dimer gap results in a sharper MD resonance in the extinction spectrum (also shown in [56]), and consequently a higher quality factor. For a small dimer gap (e.g., 4 nm), the extinction spectrum becomes broad, showing a weak MD resonance, and thus a low quality factor. The dimer gap has a significant influence on the mode volume, with a small gap providing a tightly confined electric field in the gap (see [56]); therefore, an ultra-low mode volume. On the other hand, the electric field in the gap extends further out when the dimer gap is increased. This effect results in a significant increase in mode volume. To sum up, the quality factor is low to moderate (from 3 to 16), while the mode volume can be extremely small ($< 0.005\ (\lambda/n)^3$). The Purcell factor is calculated by inserting the quality factor and mode volume in
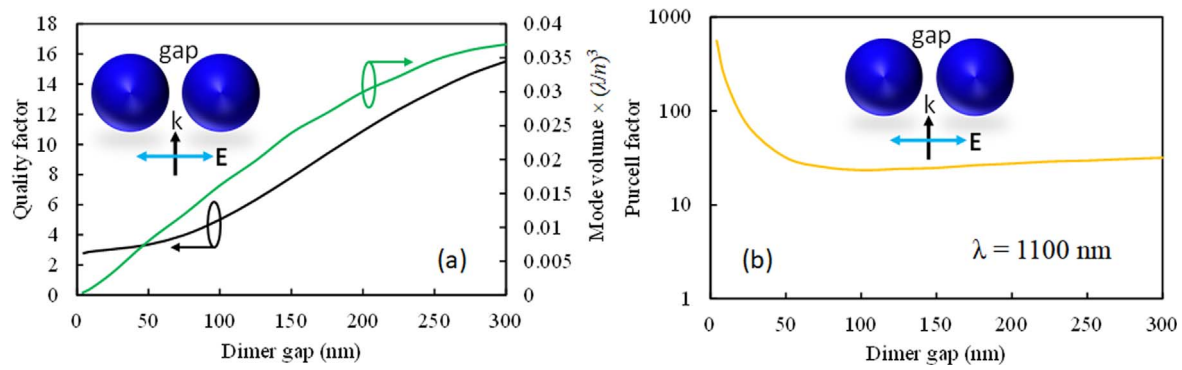
Figure 10. Simulation of a dimer to show the relationship between mode volume, quality factor and Purcell factor. The dimer consists of two Si nanospheres, radius 150 nm, separated by a gap. (a) Simulated quality-factor and mode volume as a function of dimer gap. (b) Calculated Purcell factor as a function of dimer gap at $\lambda = 1100$ nm. Schematic of the simulated dimer with excitation polarization is shown in the insets.

Table 1. Performance comparison of different dielectric nanoantennas.

| Structure	λ (nm)	Field (E/E_0)	Fluorescence	SERS	Purcell factor	Year	References
		Enhancement factor					
Si disk dimer	860	5.5	2000	1000	—	2015	[32]
Si disk dimer	633	~4.6	270	—	~20	2016	[83]
Si disk dimer	633	—	470 ± 90	1720 ± 300	—	2018	[53]
GaP disk dimer	633	~5.5	3600	—	~22	2017	[131]
GaP disk dimer	532	~6.3	—	1000	~6	2019	[133]
Si particle arrays	600	—	—	—	65	2016	[134]
Si sphere	458	—	200	—	—	2017	[135]
GaP nanodisk	700	—	—	—	~800	2019	[136]

equation (11), as shown in figure 10(b) for $\lambda = 1100$ nm. For a gap larger than 50 nm, the Purcell factor is approximately constant around 25. As the gap decreases below 50 nm, the Purcell factor increases considerably, exceeding 200 for a gap of 10 nm.

Table 1 summarizes the performance of some dielectric nanoantennas, mostly Si and GaP disk dimers. The data is limited and the table thus sparse, as can be expected for a relatively new field. The selected performance parameters are most relevant for biological applications, e.g. fluorescence and Raman-spectroscopy. Therefore, the results are for visible and near-visible wavelengths. The comparison shows that disk dimers are the most widely implemented structures for fluorescence and SERS enhancement. Field enhancement in dimer gap depends mainly on physical separation between nanoparticles, operating wavelength and refractive index of the material. The results listed in the table have different values for these parameters, thus showing different field enhancements. Fluorescence enhancement in a dimer gap is due to increased radiative emission rates. A high absorption coefficient can make a route for nonradiative decay channels, which limits the fluorescence enhancement. The absorption coefficient of GaP is one order of magnitude smaller than that of Si [131] for 633 nm, giving a negligible contribution of nonradiative decay channels. Therefore, GaP dimers provide higher fluorescence enhancement than Si dimers, as shown in table 1.

3.3. Scattering characteristics of dimers and multiple element nanoantennas

Scattering from collections of nanoparticles and arrays is a large topic and only Fano resonance and Yagi-Uda nanoantennas will be considered here. For a general treatment of scattering by small particles, see e.g. [66, 67]. Arrays of nanoantennas are considered and demonstrated in [93, 100, 102, 137].

A resonance dip found in the scattering spectrum due to the destructive interference of broad and narrow spectral lines, is known as a Fano resonance. This unique dip is sensitive to the surroundings, and can thus be used for sensing applications [138]. One way to achieve Fano resonances is the use of complex oligomer structures [99]. However, simple configurations such as Si nanoparticle dimers can also be implemented for generating a Fano resonance. When two Si nanoparticles are in close proximity, coupling between ED resonances of the two nanoparticles produces a spectrally broadened mode, while two MD resonances produce a narrow mode (figure 11(a)). Therefore, the interaction of the broad electric and the narrow magnetic modes produces a dip, i.e. a Fano resonance in the backward scattering spectrum (figure 11(b)). The Fano resonances are modified when the diameter of the two Si nanoparticles is different. Simulation and measurement of a heterodimer with diameters of 115.2 and 129.8 nm shows two Fano resonances at 511 and 592 nm, respectively (figures 11(d), (e)). Fano resonances have been
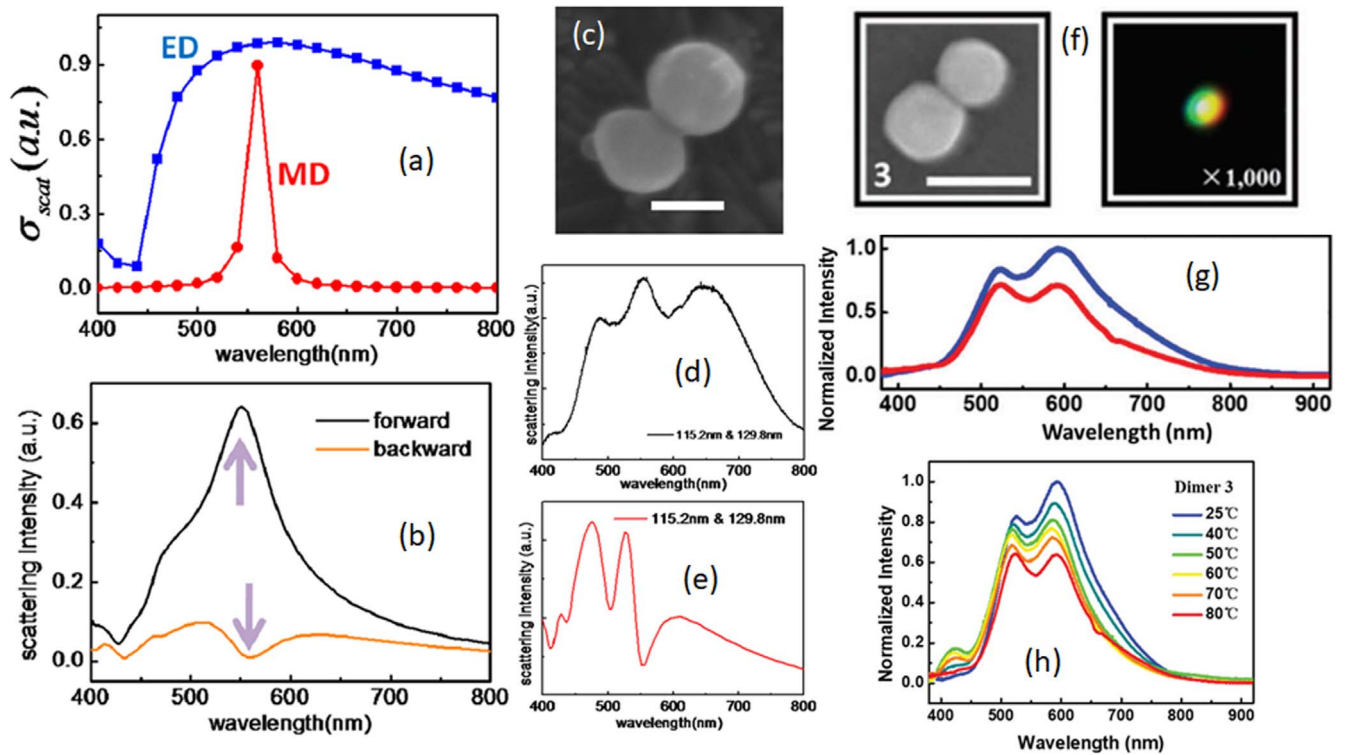
Figure 11. Fano resonances in dielectric dimers. (a) Simulated broad ED resonance and narrow MD resonance in a spherical homodimer with dimeter of 130 nm. (b) Simulated forward and backward scattering cross-sections of the homodimer. (c) SEM image of the fabricated heterodimer with dimeter of 115.2 and 129.8 nm. Backward scattering spectra found in (d) experiments and (e) numerical simulations. Reproduced with permission from [86], © 2015, ACS. (f) SEM and dark-field image of a dimer with diameter of 137.5 and 150.8 nm. (g) Experimental backward scattering intensity spectra obtained from the dimer deposited on a vanadium dioxide (VO_2) with an aluminum dioxide (Al_2O_3) substrate at 25 °C (violet curve) and 80 °C (red curve). (h) Continuous tuning of the Fano resonance by increasing temperature of the substrate. Reproduced with permission from [139], © 2019, RSC.
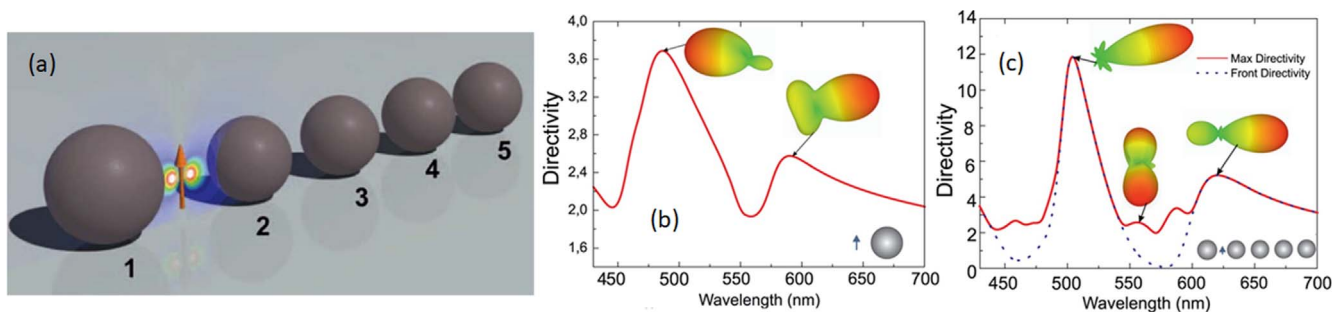

Figure 12. Yagi-Uda nanoantenna. (a) Schematic of a Si Yagi-Uda nanoantenna having a reflector with radius $R_r = 75$ nm, directors with radii $R_d = 70$ nm and excited by a point dipole. Comparison of directivity spectra for (b) a Si nanoparticle and (c) a Yagi-Uda nanoantenna. 3D radiation patterns at selected wavelengths are shown in the insets. Reproduced with permission from [44], © 2012, OSA.

demonstrated for visible wavelengths using Si dimers on a vanadium dioxide (VO_2) layer with an aluminum dioxide (Al_2O_3) substrate (figures 11(f), (g)) [139]. The resonance dips can be tuned by changing the phase transition of VO_2, which is dependent on temperature (figure 11(h)). Conversely, the temperature sensitivity makes it possible to use the nanostructure as a temperature sensor. Apart from the spherical dimers, Fano resonances have been studied recently in nanoblock dimers [140].

As discussed earlier, the radiation pattern of a single Si nanosphere can be switched from the backward to the forward direction by the Kerker effect. However, it shows low

directivity in the visible spectrum (figure 12(b)). The idea of using Yagi-Uda nanoantenna arrays (figure 12(a)) made of silicon nanospheres, was first theoretically proposed in [44]. It was numerically shown that such nanoantennas can significantly enhance the directivity compared to a single nanoparticle (figure 12(c)). Moreover, the simulations showed enhanced radiation efficiency and a higher Purcell factor compared to an Au Yagi-Uda nanoantenna. Experimentally, a Si Yagi-Uda antenna has been demonstrated for microwave frequencies [42]. For visible wavelengths, enhanced directivity has been demonstrated using a square array of Si nanodisks [100]. Recently, arrays of gallium arsenide (GaAs)
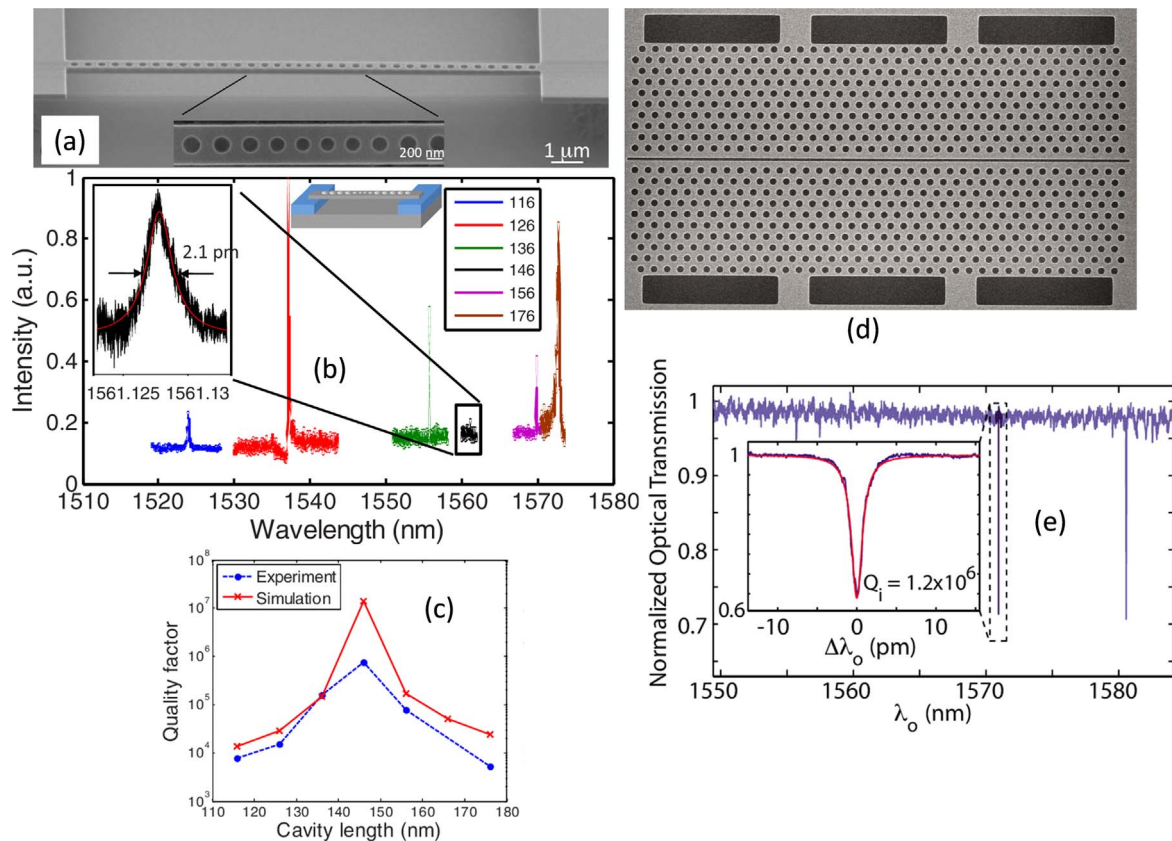
Figure 13. Optical microresonators. (a) SEM image of a fabricated photonic crystal nanobeam cavity. (b) Resonant scattering spectra for different cavity length. (c) Comparison of simulated and experimental quality-factor. Reproduced with permission from [146], © 2009, AIP. (d) SEM image of a fabricated two-dimensional slotted photonic crystal cavity. (e) Normalized optical transmission indicating the first and second order optical cavity modes. Quality-factor of the first order mode is shown in the inset. Reproduced with permission from [147], © 2010, AIP.

nanopillars have been experimentally studied for controlling the direction of emitted light, thus providing a new route for low-loss and directional lasing [93].

4. Combining dielectric optical nanoantennas and microresonators

Optical microresonators have been investigated extensively in the literature. Compared to optical nanoantennas, they provide much higher quality-factor, but at the cost of larger mode volume. A combination of microresonators and nanoantennas may thus be the ultimate combination, providing high quality-factor and small mode volume simultaneously. In this section, some recent results combining microresonators and nanoantennas will be reviewed.

Microsphere resonators have exceptionally high quality-factors, possibly the highest of any passive resonators, i.e. without amplification. As an example, a microsphere of fused silica has been demonstrated with a quality factor of 8×10^9 [141]. In addition to microspheres, a number of other designs for optical microresonators have been studied, e.g. micro-disks, micropillars, microtoroids, Fabry–Perot microcavities and photonic crystal microcavities. For reviews of optical microresonators, see [74, 142, 143]. The mode volume of a

microsphere is typically $10^3 \times (\lambda/n)^3$ [144]. Some other designs give smaller mode volume at the cost of reduced quality-factor. One example of this is a micropillar cavity made by two distributed Bragg mirrors, with a reported quality factor and mode volume of 3×10^6 and $0.1 \times (\lambda/n)^3$, respectively [145]. Furthermore, various photonic crystal structures have achieved moderate to high quality-factors, combined with the smallest mode volume among all micro-resonators. Using a one-dimensional photonic crystal nano-beam cavity in Si (shown in figure 13(a)), a quality factor of 1.4×10^7 and a mode volume of $0.39 \times (\lambda/n)^3$ were demonstrated theoretically [146]. The reported experimental quality-factor was 7.5×10^5 measured from the scattered light (shown in figure 13(c)). A two-dimensional photonic crystal cavity has been experimentally reported using a slotted structure (SEM image is shown in figure 13(d)) [147]. The measured quality-factor and simulated mode volume for the cavity were 1.2×10^6 (shown in figure 13(e)) and $0.04 \times (\lambda)^3$, respectively. The mode volume is thus comparable to that of a Si dimer (see figure 10(a)), with a significantly higher quality factor. The calculated Purcell factor is $\sim 2.3 \times 10^6$, compared to maximum a few hundred for the Si dimer. The 2D photonic crystal cavity thus outperforms the Si dimer before taking special measures.
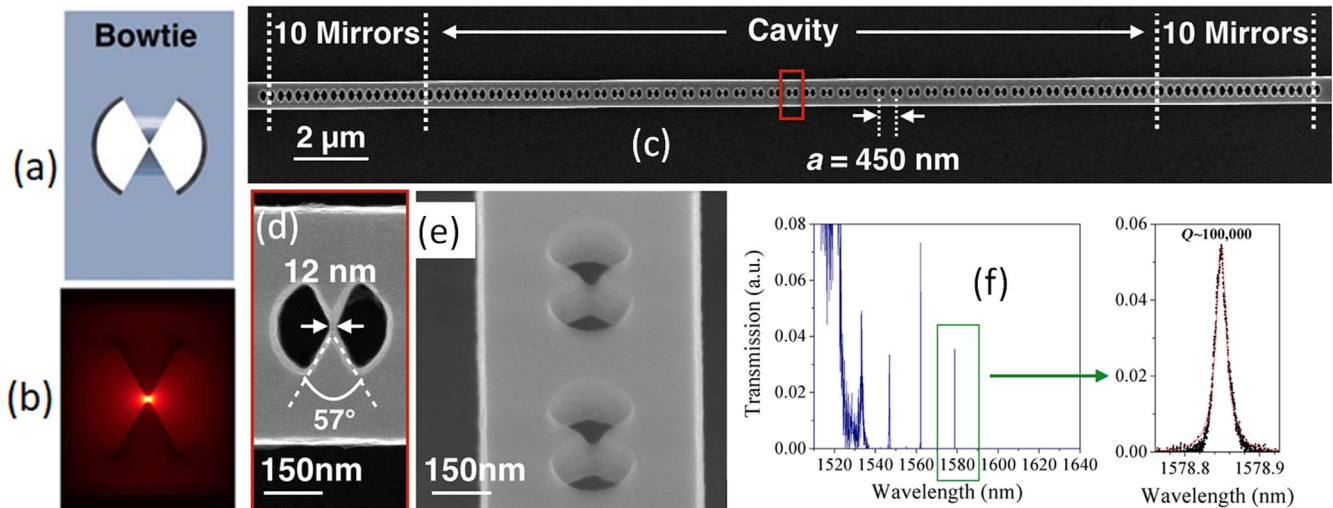
Figure. 14. Photonic crystal Si nanobeam waveguide with bowtie unit cell. (a) Schematic of the bowtie unit cell, with (b) electric energy profile. SEM images of the fabricated (c) photonic crystal cavity, (d) enlarged view of a bowtie unit cell, and (e) tilted view of the bowtie showing the partial etching. (f) Experimental transmission spectra showing optical cavity modes, with enlarged view of the fundamental mode. Reprinted/adapted from [69]. © The Authors, some rights reserved; exclusive licensee American Association for the Advancement of Science. Distributed under a Creative Commons Attribution NonCommercial License 4.0 (CC BY-NC).

Microspheres have been combined with plasmonic nanoantennas [148–150]. In principle, several of the micro-resonator-designs can be combined with dielectric optical nanoantennas. Adding a nanoantenna to a microresonator will increase the loss if the nanoantenna is not perfectly matched to the mode of the microresonator, even if the nanoantenna does not have intrinsic losses. Perfect mode-matching is difficult to achieve for most microresonator-designs. As an example, fixing a Si dimer to the surface of a microsphere will give scattering and thus reduce the quality-factor of the microsphere. For waveguide ring resonators, an adiabatic transition to a nanoantenna etched into the waveguide core can be imagined. Going one step further, it has been proposed to embed a bowtie antenna in the unit cell of a photonic crystal waveguide [71]. This can give extreme light concentration at the bowtie tip as shown in figure 14(b) and thus provides an ultra-low mode volume. According to simulations, the bowtie unit cell provides 80 times enhancement of the peak electric field amplitude compared to a traditional circular unit cell [69]. The proposed design has been made and experimentally validated by S Hu *et al* [69], which is shown in figures 14(c)–(f). Note the small dimensions of the bowtie unit cell, with a minimum width of 12 nm (figure 14(d)). As the gap in the bowtie is not completely etched away (figure 14(e)), the mode volume is further reduced. The measured quality-factor was $\sim10^5$, with a (simulated) mode volume of $10^{-3} \times (\lambda/n)^3$. This combination gives a Purcell factor of $\sim8 \times 10^6$.

The combination of nanoantennas with resonators can thus give extremely high Purcell factors. This may result in significant improvements for applications such as optical trapping, as predicted in [151]. The combination may also find other applications, e.g. for single-molecule fluorescence and Raman-spectroscopy of nanoparticles. However, the wavelength of the emitter (or absorber) must be closely matched to the resonance wavelength of the resonator. Also, the combination is suitable for one or a few nanoantennas, as opposed to single nanospheres, which can easily be multiplied to very large numbers. Combining nanoantennas and micro-resonators thus give very interesting results for applications where the wavelength can be adapted to the resonator and where a limited number of nanoantennas is required.

## 5. Applications of dielectric nanoantennas

Optical nanoantennas can be utilized in various applications including optical trapping [83, 132, 152], spectroscopy [31, 32, 131, 135], photovoltaics [153], directional lasing [93], nonlinear signal conversion [154–160] and optical sensing [161, 162]. A few of them have already been employed as operational devices (e.g. on-chip biosensing [101]), while others are expected to be implemented in devices soon (e.g. directional lasing [93]). In this section, we will discuss a few emerging applications.

5.1. Optical trapping

The application of dielectric optical nanoantennas to optical trapping is highly promising. The main reasons are low local heating and strong electric and magnetic resonances. Conventional optical tweezers can trap micrometer-sized particles by using the optical forces exerted from highly focused laser beams [163]. Their application to trapping of nanoparticles is limited because the trapping relies on the gradient force, which scales with the volume of the particle [164]. As lenses are used in the trapping system, the focal spot and thus the gradient forces are limited by the diffraction limit. Therefore, there is a lower limit for the size of a particle that can be trapped, depending on its refractive index, input power, and to some extent the shape of the particle. Dielectric nanoantennas

14
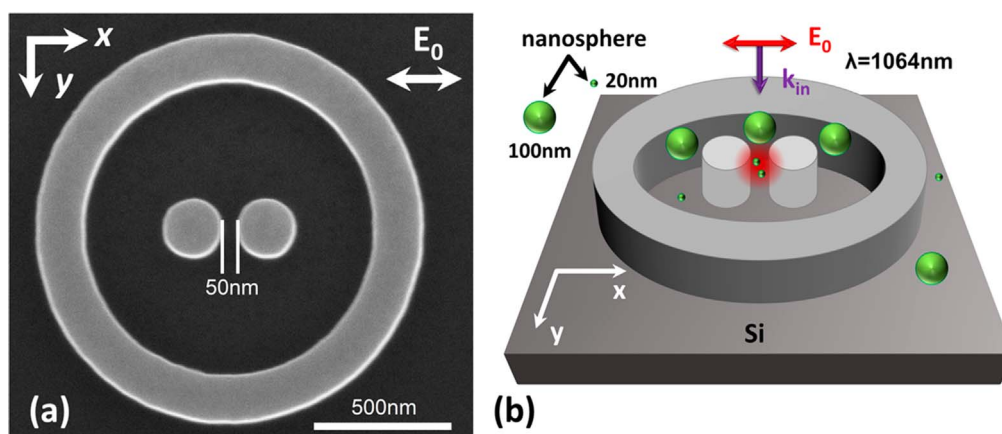
Figure 15. Si dimers for nanoparticle trapping. (a) SEM image of the fabricated silicon optical nanoantenna placed on a silicon substrate (top view) (b) Schematic of the optical trapping of nanospheres of diameter 20, while 100 nm nanospheres are not trapped. Reproduced with permission from [132], © 2018, ACS.
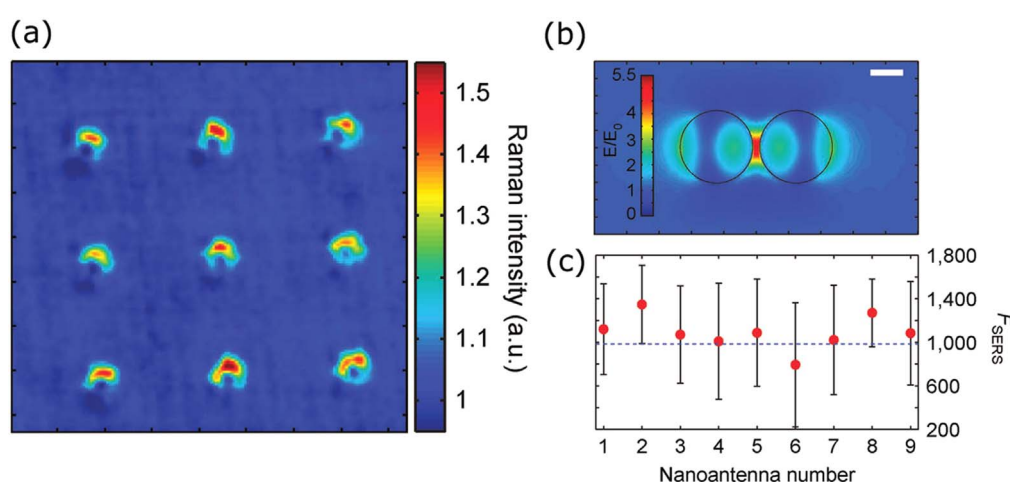
Figure 16. Surface-enhanced Raman scattering with silicon dimers. (a) Map of measured Raman-intensity for nine similar silicon dimers. (b) Simulated electric field enhancement for 20 nm gap between the silicon disks, and (c) SERS enhancement factors for the nine nanoantennas and the expected value (dotted line). Reproduced with permission from [32], © 2015, Nature Publishing Group.

can provide an effective solution to overcome this limit. Similarly to plasmonic nanoantennas, dielectric nanoantennas can be used to confine light to sub-wavelength mode volumes and thus enhance the gradient forces. This can be used for stable trapping of nanoparticles with low optical power. As dielectric nanoantennas produce less Joule heating than plasmonic ones, there is less thermally induced flow around the nanoantenna, which can push particles away. Also, avoiding heating is particularly important for some biological applications [165]. Recently, silicon optical nanoantennas have been reported for trapping of polystyrene nanospheres [132]. The authors used a pair of silicon nanocylinders having a gap of 50 nm and were able to trap multiple nanospheres with diameters of 20 nm (see figure 15). A single streptavidin-coated CdSe/ZnS quantum dot was trapped with similar dielectric nanoantennas in [152].

5.2. Surface-enhanced spectroscopy and fluorescence

Two other emerging applications of dielectric nanoantennas are surface-enhanced Raman spectroscopy (SERS) [32, 166, 167]

and surface-enhanced fluorescence emission [32, 131]. As for optical trapping, nanoantennas improve the light–matter inter-actions through tightly localizing the optical field. This increases the Purcell factor and improves excitation rates [40], which translates into larger Raman-scattering and increased fluorescence from material in the nanocavity. Due to less local heating, high Purcell factors, and improvement of the radiative decay rate, single-molecule sensitivity has been demonstrated with dielectric nanoantennas, as for plasmonic nanoantennas [83]. It has been shown that silicon nanoantennas provide better quantum efficiency than the plasmonic nanoantennas [56]. Dielectric dimer nanoantennas were used in [32] for producing surface-enhanced fluorescence and SERS. The measured Raman-intensity is shown in figure 16(a), where nine similar silicon dimers were demonstrated. Due to the enhancement of the near-field (figure 16(b)), the dimer nanoantennas showed an increase in the Raman scattering by a factor of 1000 (figure 16(c)).

Dielectric nanoantennas are free from quenching and charge carriers [165]. An emitter, in nanometer proximity of a

plasmonic structure, can be quenched due to nonradiative decay channels. This can be avoided by using dielectric spacers for plasmonic structures, while for dielectric nanoantennas, the problem is avoided entirely. This is a key benefit for dielectric nanoantennas as opposed to plasmonic nanoantennas. Using single silicon dielectric nanospheres, the fluorescence signal from a dye has been enhanced 200 times without a dielectric spacer [135]. Using a silicon dimer with a gap of 20 nm, 270-fold enhancement of a fluorescence signal has been demonstrated [131]. In another work on gallium phosphide (GaP) dimers [83], the authors reported 3600 times enhancement of the fluorescence signal.

5.3. Nonlinear photonics

Dielectric nanoantennas have gained attention for increasing photon–photon interactions. They are considered building blocks for exploring nonlinear effects because of low losses and the coexistence of both electric and magnetic resonances [154]. This is in contrast to plasmonic nanoantennas, which are dominated by electric resonances. Nonlinear optical effects can have very different properties depending on whether their origin is magnetic or electric. When the electric and magnetic resonances are mixed, nonlinear properties change considerably. This leads to new applications in nanophotonics such as nonlinear mode-mixing [168]. Recently, nonlinear effects have been studied, including second-harmonic generation (SHG) [155, 157, 160] and third-harmonic generation (THG) [154, 156, 158, 169], using dielectric nanoantennas. Such nonlinear effects find important applications in bioimaging and biosensing [170, 171]. Unfortunately, silicon nanoantennas for nonlinear effects areof limited use for optical communications, due to two-photon absorption. A practical solution is to use III-V materials, e.g. AlGaAs, which can be made transparent in the visible range. Thus, two-photon absorption is avoided and the materials are suitable for investigating nonlinear effects such as SHG. SHG based on AlGaAs nanodisks has been reported in [155, 160]. Additionally, germanium nanodisks have been explored for THG [154].

5.4. Solar cells

High-efficiency solar cells are required for sustainable and environmentally-friendly energy production. One of the key strategies to improve the efficiency of solar cells is to increase the solar absorption by light trapping [153]. Several nanoantenna structures have been demonstrated [153, 172, 173] for this application. An one dimensional (1D) dielectric core–shell nanoantennas made of absorbing amorphous silicon and nonabsorbing ZnO and Si_3N_4 have been reported to enhance the solar absorption [153]. Moreover, Si nanowires coated with dielectric shells and nanocrystalline Si nanoshells were also explored for enhanced light absorption [173, 174]. Additionally, submicron spherical Si arrays and Ge nanopillar arrays have been demonstrated for enhancement of the solar absorption [172, 175].

6. Dielectric materials and fabrication technologies

To obtain tight confinement of light in a nanoantenna, the material must have a high refractive index. The material should also have moderate or low losses from absorption, and preferably a low cost. As the size of the device is small, higher losses and cost can be accepted than for larger devices, e.g. a waveguide crossing a cm size chip. An extinction coefficient $k = 0.01$ can be used to demonstrate this difference. For a nanoantenna with dimensions similar to the wavelength (e.g. $\lambda_0 = 1\,\mu m$), $k = 0.01$ corresponds to ~ 0.5 dB propagation loss, which might be an acceptable value. However, if the loss is due to absorption, the nanoantenna might heat up for a modest input power, and one of the main advantages of dielectrics over plasmonics is thus lost. Also, if the nanoantenna is to be combined with a resonator, the losses for the resonator material must be very low to get a high quality-factor. This can be done by combining two materials, a low-loss material for the resonator and a material with high refractive index for the nanoantenna. As losses depend on the wavelength, the choice of material depends on the wavelength required for the application. Finally, the availability of a suitable fabrication method can influence the choice of material for a nanoantenna.

Table 2 lists some relevant materials and includes both dielectrics and semiconductors. The properties of the materials depend strongly on wavelength, particularly close to absorption edges, and also depend on the fabrication method. Impurities can increase the extinction coefficient significantly and a porous structure can have a lower refractive index than a dense one. Values for the wavelength range are set to match the given (maximum) extinction coefficients. The values for the extinction coefficient are in several cases indicated as zero ($k \sim 0$), showing that the value is limited by the measurement range rather than the material. Some of the listed values have been measured for bulk materials and some are from models, and the values should thus be treated critically when used for designing nanostructures.

Silicon is a widely-used semiconductor material with low cost and mature fabrication technology [187]. It has a high refractive index and is very suitable for nanoantennas in the near-infrared, e.g. for telecommunications, and most of the examples in this review are on silicon nanoantennas. For biological applications, e.g. surface-enhanced Raman spectroscopy and fluorescence, visible light is mostly used. As silicon is partially absorbing for visible wavelengths, it can be used for small structures, i.e. the nanoantenna itself, operating in the visible. Some amorphous materials are transparent in the visible and have a moderately high refractive index, notably SiN/Si_3N_4, Ta_2O_5 and TiO_2. Amorphous materials can be deposited with common deposition methods, e.g. low pressure and plasma-enhanced chemical vapor deposition (LPCVD and PECVD), magnetron sputtering and atomic layer deposition. As the deposition is typically done on top of a silicon wafer, the cost is low compared to materials that need a crystalline wafer of the same material-type. For higher refractive index, a few crystalline semiconductor materials are transparent in the visible/NIR-range, e.g.

Table 2. Some relevant dielectric and semiconductor materials for optical nanoantennas. Most values have been accessed through [176].

Material	Spectral range (μm)	Refractive index (n)	Extinction coefficient (k)	References
TiO$_2$	0.4–1.7	2.34–2.05	$\sim$0	[177]
Ta$_2$O$_5$	0.5–1.8	2.2–2.1	$\sim$0	[178]
Si$_3$N$_4$	0.5–2.5	2.1–2	$\sim$0	[179]
c-Si	0.5–1.1	4.3–3.5	0.049–3×10^{-5}	[180]
	1.1–8.3	3.5–3.4	$<3 \times 10^{-5}$	[181]
SiC	1–7.5	3.3–2.9	<0.1	[182]
AlGaAs	0.75–12	3.6–3	<0.02	[183, 184]
Ge	1.1–1.8	4.3–4.1	<0.01	[185]
	1.8–11	4.1–4	$\sim$0	[185]
GaSb	1.5–12	4–3.7	<0.1	[184]
Te	1.6–2	4.5–4.3	<0.1	[186]
GaP	0.5–12	3.6–3.1	<0.01	[184]

AlGaAs and GaP. For high refractive index in the mid- and far-IR, germanium, antimonides, tellurides, and silicon carbide are attractive and have low extinction coefficient. The cost would be high for a large wafer with these materials, but a wafer can contain a very large number of nanoantennas. Thus, the cost can be acceptable and even low for highly efficient devices, e.g. consisting of a few nanowires or nanospheres. For devices that can be separated from the crystalline wafer used for fabrication, hybrid integration on a silicon wafer with other optical devices is an option.

Fabrication techniques for optical nanoantennas include methods for thin-film deposition and patterning [188], growth of nanowires [189], and chemical methods for synthesis of nanoparticles [190]. A review of materials and fabrication methods for dielectric nanophotonics can be found in [1]. The choice of method is directly linked to the choice of material, and adapting and optimizing a technique for a new material can be a significant task. Passing from the research-stage to making components in a foundry is a big leap, and here silicon photonics has a large advantage. There are several foundries that make silicon photonics and compatible materials, e.g. S$_3$N$_4$ [191–194]. For nanoantennas made with non-standard materials, nanowires and nanoparticles, hybrid integration with silicon photonic circuits can be an alternative, as it is for quantum photonics [195]. Solar cells are an important, large-scale application of optical nanoantennas. Fabrication challenges and cost-issues are, due to the scale, very different from applications that focus on one or a few components, with a finite number of nanoantennas.

7. Discussion and outlook

This review provides a brief overview of recent advances regarding dielectric optical nanoantennas. It presents a broad classification based on the structural configuration of the nanoantennas and provides a review of selected works in each category. As an example, original simulation results are included for a spherical silicon dimer, quantifying parameters that are relevant for optical nanoantennas, such as mode volume, quality factor, and Purcell factor. The example shows that the nanoantenna has a very small mode volume, but on its own it has a modest quality factor. This is a typical feature of optical nanoantennas as it is difficult to make a nano-size cavity with high quality-factor. There are a number of options for making high quality-factor optical resonators, both microresonators and larger, e.g. waveguide resonators. By combining nanoantennas with resonators, both very small mode volume and very high quality-factor can be obtained, as recently demonstrated [69]. The combination of dielectric optical nanoantennas and high quality-factor resonators is very promising, with performance set to improve and applications multiply in the future.

Low heat generation is one of the main advantages of dielectric optical nanoantennas, as compared to plasmonics. This is particularly important for applications with high power or when a nanoantenna is combined with a resonator, and also for some biological applications where temperature must be kept stable. Whereas plasmonics has established methods and designs to handle heating, the focus for dielectrics has mostly been on reducing dissipative loss in the materials. There are thus lessons to be learned from plasmonics, as for other topics related to the functioning of optical nanoantennas. Scattering losses are less important for nanostructures as they will not accumulate over a long structure, which is the case for e.g. optical waveguides. However, scattering and unintended hotspots might compromise the intended function of the nanoantenna and making perfectly smooth surfaces is a challenge. Whereas characterization of smoothness can readily be done with profilers and atomic force microscopes on the wafer- and chip-level, it is far from trivial to do the same for nanoantennas that have features in the nm range, and that can be very thin or have a spherical shape.

Silicon is dominating the field of dielectric nanoantennas, as can be expected from its excellent optical, thermal and mechanical properties, and its mature fabrication technology inherited from microelectronics. For near- to mid-IR, Si is highly transparent and has a high refractive index. For biological applications, e.g. Raman spectroscopy and fluorescence, visible wavelengths are preferable. Here, silicon has a disadvantage due to some absorption. Thus, other materials

can be good alternatives, both amorphous dielectrics (e.g. SiN, Ta$_2$O$_5$, TiO$_2$) with a lower refractive index, and other semiconductors (e.g. GaP, AlGaAs). Biology will probably be a major application for optical nanoantennas in the future, and many optical functions can be imagined, e.g. various types of super-resolution microscopy with nanoantennas. Thus, there is a need for new materials with a high refractive index and new designs of optical nanoantennas, suitable for biological applications in the visible range. The UV range has not been considered in this review. It is currently attracting attention, e.g. for nonlinear optics [196], and as the wavelength gets shorter, it might give an even smaller mode volume than for the visible range. For wavelengths approaching the UV-absorption edge of a material, the increased loss is accompanied by an increase in the refractive index. A compromise between refractive index and loss must thus be made, which can work well for nanoantennas. There is a limited number of suitable materials for the UV range, and new materials might become available if the interest increases. For existing materials, improving the purity, fabrication methods and characterization will be beneficial for the scientific community and for all wavelength ranges. The combination of optical functions, e.g. nanoantennas and microresonators, and further combination with nonoptical functions, e.g. microfluidics, thermal control and electric circuits, all on one chip, can open entirely new applications. Hybrid integration with detectors, lasers and other sources, is also of great interest, and can lead to highly efficient and cost-effective nanophotonic systems.

ORCID iDs

Md Rabiul Hasan ● https://orcid.org/0000-0002-9538-454X
Olav Gaute Hellesø ● https://orcid.org/0000-0002-0494-8240

References

[1] Baranov D G *et al* 2017 All-dielectric nanophotonics: the quest for better materials and fabrication techniques *Optica* **4** 814–25

[2] Kang J-H *et al* 2011 Low-power nano-optical vortex trapping via plasmonic diabolo nanoantennas *Nat. Commun.* **2** 582

[3] Righini M *et al* 2009 Nano-optical trapping of Rayleigh particles and *Escherichia coli* bacteria with resonant optical antennas *Nano Lett.* **9** 3387–91

[4] Roxworthy B J *et al* 2012 Application of plasmonic bowtie nanoantenna arrays for optical trapping, stacking, and sorting *Nano Lett.* **12** 796–801

[5] Law S *et al* 2013 All-semiconductor plasmonic nanoantennas for infrared sensing *Nano Lett.* **13** 4569–74

[6] Liu N *et al* 2011 Nanoantenna-enhanced gas sensing in a single tailored nanofocus *Nat. Mater.* **10** 631–6

[7] Tittl A *et al* 2012 Spectral shifts in optical nanoantenna-enhanced hydrogen sensors *Opt. Mater. Express* **2** 111–8

[8] Zundel L and Manjavacas A 2017 Spatially resolved optical sensing using graphene nanodisk arrays *ACS Photonics* **4** 1831–8

[9] Pfeiffer M *et al* 2014 Eleven nanometer alignment precision of a plasmonic nanoantenna with a self-assembled GaAs quantum dot *Nano Lett.* **14** 197–201

[10] Ridolfo A *et al* 2010 Quantum plasmonics with quantum dot-metal nanoparticle molecules: influence of the Fano effect on photon statistics *Phys. Rev. Lett.* **105** 263601

[11] Hou J *et al* 2014 Dissipation-driven entanglement between qubits mediated by plasmonic nanoantennas *Phys. Rev.* B **89** 235413

[12] Alù A and Engheta N 2010 Wireless at the nanoscale: optical interconnects using matched nanoantennas *Phys. Rev. Lett.* **104** 213902

[13] Ahmed A and Gordon R 2011 Directivity enhanced Raman spectroscopy using nanoantennas *Nano Lett.* **11** 1800–3

[14] Neubrech F *et al* 2017 Surface-enhanced infrared spectroscopy using resonant nanoantennas *Chem. Rev.* **117** 5110–45

[15] Pucci A *et al* 2010 Surface enhanced infrared spectroscopy using gold nanoantennas *Phys. Status Solidi* (B) **247** 2071–4

[16] D'Andrea C *et al* 2013 Optical nanoantennas for multiband surface-enhanced infrared and Raman spectroscopy *ACS Nano* **7** 3522–31

[17] Estrada L C, Aramendía P F and Martínez O E 2008 10000 times volume reduction for fluorescence correlation spectroscopy using nano-antennas *Opt. Express* **16** 20597–602

[18] Chen P-Y, Argyropoulos C and Alù A 2012 Enhanced nonlinearities using plasmonic nanoantennas *Nanophotonics* **1** 221–33

[19] Biagioni P, Huang J-S and Hecht B 2012 Nanoantennas for visible and infrared radiation *Rep. Prog. Phys.* **75** 024402

[20] Obermeier J, Schumacher T and Lippitz M 2018 Nonlinear spectroscopy of plasmonic nanoparticles *Adv. Phys.* X **3** 1454341

[21] Giannini V *et al* 2011 Plasmonic nanoantennas: fundamentals and their use in controlling the radiative properties of nanoemitters *Chem. Rev.* **111** 3888–912

[22] Berkovitch N, Ginzburg P and Orenstein M 2012 Nano-plasmonic antennas in the near infrared regime *J. Phys. Condens. Matter* **24** 073202

[23] Christos A *et al* 2015 Plasmonic nanoantennas: enhancing light–matter interactions at the nanoscale *EPJ Appl. Metamater.* **2** 4

[24] Krasnok A E *et al* 2013 Optical nanoantennas *Phys.-Usp.* **56** 539–64

[25] Sheverdin A and Valagiannopoulos C 2019 core–shell nanospheres under visible light: optimal absorption, scattering, and cloaking *Phys. Rev.* B **99** 075305

[26] Tzarouchis D C and Sihvola A 2018 General scattering characteristics of resonant core–shell spheres *IEEE Trans. Antennas Propag.* **66** 323–30

[27] Arslanagić S and Jacobsen R E 2019 Active coated nano rod antennas for enhanced and directive scattering phenomena *EPJ Appl. Metamater.* **6** 19

[28] Valagiannopoulos C A 2007 Single-series solution to the radiation of loop antenna in the presence of a conducting sphere *Prog. Electromagn. Res.* **71** 277–94

[29] Thorsen R and Arslanagić S 2015 Eccentrically-layered active coated nano-particles for directive near- and far-field radiation *Photonics* **2** 773–94

[30] Campbell S D and Ziolkowski R W 2015 Near-field directive beams from passive and active asymmetric optical nanoantennas *IEEE J. Sel. Top. Quantum Electron.* **21** 312–23

[31] Albella P *et al* 2014 Electric and magnetic field enhancement with ultralow heat radiation dielectric nanoantennas: considerations for surface-enhanced spectroscopies *ACS Photonics* **1** 524–9

[32] Caldarola M *et al* 2015 Non-plasmonic nanoantennas for surface enhanced spectroscopies with ultra-low heat conversion *Nat. Commun.* **6** 7915

[33] Barreda A I *et al* 2019 Recent advances in high refractive index dielectric nanoantennas: basics and applications *AIP Adv.* **9** 040701

[34] Guo H *et al* 2013 Near-field focusing of the dielectric microsphere with wavelength scale radius *Opt. Express* **21** 2434–43

[35] Heifetz A *et al* 2007 Subdiffraction optical resolution of a gold nanosphere located within the nanojet of a Mie-resonant dielectric microsphere *Opt. Express* **15** 17334–42

[36] Teraoka I, Arnold S and Vollmer F 2003 Perturbation approach to resonance shifts of whispering-gallery modes in a dielectric microsphere as a probe of a surrounding medium *J. Opt. Soc. Am.* B **20** 1937–46

[37] Rodriguez I *et al* 2014 Silicon nanoparticles as Raman scattering enhancers *Nanoscale* **6** 5666–70

[38] Krasnok A E *et al* 2014 Superdirective dielectric nanoantennas *Nanoscale* **6** 7354–61

[39] Zywietz U *et al* 2014 Laser printing of silicon nanoparticles with resonant optical electric and magnetic responses *Nat. Commun.* **5** 3402

[40] Rolly B *et al* 2012 Promoting magnetic dipolar transition in trivalent lanthanide ions with lossless Mie resonances *Phys. Rev.* B **85** 245432

[41] Dregely D *et al* 2011 3D optical Yagi–Uda nanoantenna array *Nat. Commun.* **2** 267

[42] Filonov D S *et al* 2012 Experimental verification of the concept of all-dielectric nanoantennas *Appl. Phys. Lett.* **100** 201113

[43] Ghanim A M *et al* 2016 Highly directive hybrid yagi-uda nanoantenna for radition emission enhancement *IEEE Photonics J.* **8** 5501712

[44] Krasnok A E *et al* 2012 All-dielectric optical nanoantennas *Opt. Express* **20** 20599–604

[45] Krasnok A E *et al* 2011 Huygens optical elements and Yagi—Uda nanoantennas based on dielectric nanoparticles *JETP Lett.* **94** 593–8

[46] Tsuchimoto Y *et al* 2016 Fano resonant all-dielectric core/shell nanoparticles with ultrahigh scattering directionality in the visible region *Opt. Express* **24** 14451–62

[47] Li R *et al* 2018 Broadband zero backward scattering by all-dielectric core–shell nanoparticles *Opt. Express* **26** 28891–901

[48] de Sousa N *et al* 2016 Magneto-optical activity in high index dielectric nanoantennas *Sci. Rep.* **6** 30803

[49] Baranov D G *et al* 2016 Tuning of near- and far-field properties of all-dielectric dimer nanoantennas via ultrafast electron-hole plasma photoexcitation *Laser Photonics Rev.* **10** 1009–15

[50] Shibanuma T, Albella P and Maier S A 2016 Unidirectional light scattering with high efficiency at optical frequencies based on low-loss dielectric nanoantennas *Nanoscale* **8** 14184–92

[51] Shibanuma T *et al* 2017 Experimental demonstration of tunable directional scattering of visible light from all-dielectric asymmetric dimers *ACS Photonics* **4** 489–94

[52] Albella P, Shibanuma T and Maier S A 2015 Switchable directional scattering of electromagnetic radiation with subwavelength asymmetric silicon dimers *Sci. Rep.* **5** 18322

[53] Cambiasso J *et al* 2018 Surface-enhanced spectroscopies of a molecular monolayer in an all-dielectric nanoantenna *ACS Photonics* **5** 1546–57

[54] Lapshina N, Noskov R and Kivshar Y 2012 Nanoradar based on nonlinear dimer nanoantenna *Opt. Lett.* **37** 3921–23

[55] Zywietz U *et al* 2015 Electromagnetic resonances of silicon nanoparticle dimers in the visible *ACS Photonics* **2** 913–20

[56] Albella P *et al* 2013 Low-loss electric and magnetic field-enhanced spectroscopy with subwavelength silicon dimers *J. Phys. Chem.* C **117** 13573–84

[57] Gómez F R, Mejía-Salazar J R and Albella P 2019 All-dielectric chiral metasurfaces based on crossed-bowtie nanoantennas *ACS Omega* **4** 21041–7

[58] Valagiannopoulos C A *et al* 2014 Hyperbolic-metamaterial antennas for broadband enhancement of dipole emission to free space *J. Appl. Phys.* **116** 163106

[59] Valagiannopoulos C A and Sihvola A 2013 Improving the electrostatic field concentration in a negative-permittivity wedge with a grounded 'bowtie' configuration *Radio Sci.* **48** 316–25

[60] Zhang X M *et al* 2018 Dual-band unidirectional forward scattering with all-dielectric hollow nanodisk in the visible *Opt. Lett.* **43** 1275–78

[61] Visser D *et al* 2019 Optical properties and fabrication of dielectric metasurfaces based on amorphous silicon nanodisk arrays *Opt. Express* **27** 5353–67

[62] Lv J *et al* 2018 Multi-wavelength unidirectional forward scattering in the visible range in an all-dielectric silicon hollow nanodisk *Appl. Opt.* **57** 4771–76

[63] Frolov A Y *et al* 2017 Near-field mapping of optical fabry–perot modes in all-dielectric nanoantennas *Nano Lett.* **17** 7629–37

[64] Abujetas D R *et al* 2017 High-contrast fano resonances in single semiconductor nanorods *ACS Photonics* **4** 1814–21

[65] Novotny L and van Hulst N 2011 Antennas for light *Nat. Photonics* **5** 83–90

[66] Mishchenko M I, Travis L D and Lacis A A 2002 *Scattering, Absorption, and Emission of Light by Small Particles* (Cambridge: Cambridge University Press)

[67] Bohren C F and Huffman D R 1998 *Absorption and Scattering of Light by Small Particles* (New York: Wiley) (https://doi.org/10.1002/9783527618156)

[68] Bharadwaj P, Deutsch B and Novotny L 2009 Optical antennas *Adv. Opt. Photonics* **1** 438–83

[69] Hu S *et al* 2018 Experimental realization of deep-subwavelength confinement in dielectric optical resonators *Sci. Adv.* **4** eaat2355

[70] Altug H, Englund D and Vučković J 2006 Ultrafast photonic crystal nanocavity laser *Nat. Phys.* **2** 484–8

[71] Hu S and Weiss S M 2016 Design of photonic crystal cavities for extreme light concentration *ACS Photonics* **3** 1647–53

[72] Landau L D and Lifshitz E M 1974 *Quantum Mechanics* (Pergamon) ch 4 116–35

[73] Purcell E M, Torrey H C and Pound R V 1946 Resonance absorption by nuclear magnetic moments in a solid *Phys. Rev.* **69** 37–8

[74] Vahala K J 2003 Optical microcavities *Nature* **424** 839–46

[75] Jiao X and Blair S 2012 Optical antenna design for fluorescence enhancement in the ultraviolet *Opt. Express* **20** 29909–22

[76] Sun G and Khurgin J B 2012 Origin of giant difference between fluorescence, resonance, and nonresonance Raman scattering enhancement by surface plasmons *Phys. Rev.* A **85** 063410

[77] Maslovski S I and Simovski C R 2019 Purcell factor and local intensity enhancement in surface-enhanced Raman scattering *Nanophotonics* **8** 429–34

[78] Zhao X and Reinhard B M 2019 Switchable chiroptical hot-spots in silicon nanodisk dimers *ACS Photonics* **6** 1981–9

[79] Rolly B *et al* 2013 Controllable emission of a dipolar source coupled with a magneto-dielectric resonant subwavelength scatterer *Sci. Rep.* **3** 3063

[80] Todisco F *et al* 2020 Magnetic and electric Mie-exciton polaritons in silicon nanodisks *Nanophotonics* **9** 803–14

[81] Feng T *et al* 2018 Unidirectional emission in an all-dielectric nanoantenna *J. Phys. Condens. Matter* **30** 124002

[82] Habteyes T G *et al* 2014 Near-field mapping of optical modes on all-dielectric silicon nanodisks *ACS Photonics* **1** 794–8

[83] Regmi R *et al* 2016 All-dielectric silicon nanogap antennas to enhance the fluorescence of single molecules *Nano Lett.* **16** 5143–51

[84] Fu D *et al* 2017 Polarization-selective optical resonance with extremely narrow linewidth in Si dimers array for application in ultra-sensitive refractive sensing *Opt. Commun.* **390** 41–8

[85] Wang H *et al* 2015 Janus Magneto–electric nanosphere dimers exhibiting unidirectional visible light scattering and strong electromagnetic field enhancement *ACS Nano* **9** 436–48

[86] Yan J *et al* 2015 Directional fano resonance in a silicon nanosphere dimer *ACS Nano* **9** 2968–80

[87] Deng F *et al* 2018 Sharp bending and power distribution of a focused radially polarized beam by using silicon nanoparticle dimers *Opt. Express* **26** 20051–62

[88] Das T and Schuller J A 2017 Dark modes and field enhancements in dielectric dimers illuminated by cylindrical vector beams *Phys. Rev.* B **95** 201111(R)

[89] Jia Z-Y *et al* 2016 Dipole coupling and dual Fano resonances in a silicon nanodimer *J. Appl. Phys.* **119** 074302

[90] Wang L *et al* 2017 Shaping the third-harmonic radiation from silicon nanodimers *Nanoscale* **9** 2201–6

[91] Mirzaei A and Miroshnichenko A E 2015 Electric and magnetic hotspots in dielectric nanowire dimers *Nanoscale* **7** 5963–8

[92] Černigoj J *et al* 2018 Lattice resonances and local field enhancement in array of dielectric dimers for surface enhanced Raman spectroscopy *Sci. Rep.* **8** 15706

[93] Ha S T *et al* 2018 Directional lasing in resonant semiconductor nanoantenna arrays *Nat. Nanotechnol.* **13** 1042–7

[94] Liu Y G *et al* 2012 Unidirectional and wavelength-selective photonic sphere-array nanoantennas *Opt. Lett.* **37** 2112–4

[95] Filonov D S *et al* 2014 Near-field mapping of Fano resonances in all-dielectric oligomers *Appl. Phys. Lett.* **104** 021104

[96] Shcherbakov M R *et al* 2015 Nonlinear interference and tailorable third-harmonic generation from dielectric oligomers *ACS Photonics* **2** 578–82

[97] Hopkins B *et al* 2015 Interplay of magnetic responses in all-dielectric oligomers to realize magnetic fano resonances *ACS Photonics* **2** 724–9

[98] Yan J H *et al* 2015 Magnetically induced forward scattering at visible wavelengths in silicon nanosphere oligomers *Nat. Commun.* **6** 7042

[99] Miroshnichenko A E and Kivshar Y S 2012 Fano resonances in all-dielectric oligomers *Nano Lett.* **12** 6459–63

[100] Vaskin A *et al* 2018 Directional and spectral shaping of light emission with mie-resonant silicon nanoantenna arrays *ACS Photonics* **5** 1359–64

[101] Yavas O *et al* 2017 On-a-chip biosensing based on all-dielectric nanoresonators *Nano Lett.* **17** 4421–6

[102] Chong K E *et al* 2014 Observation of fano resonances in all-dielectric nanoparticle oligomers *Small* **10** 1985–90

[103] Kuznetsov A I *et al* 2016 Optically resonant dielectric nanostructures *Science* **354** aag2472

[104] Sain B, Meier C and Zentgraf T 2019 Nonlinear optics in all-dielectric nanoantennas and metasurfaces: a review *Adv. Photonics* **1** 024002

[105] Evlyukhin A B *et al* 2010 Optical response features of Si-nanoparticle arrays *Phys. Rev.* B **82** 045404

[106] García-Etxarri A *et al* 2011 Strong magnetic response of submicron Silicon particles in the infrared *Opt. Express* **19** 4815–26

[107] Kuznetsov A I *et al* 2012 Magnetic light *Sci. Rep.* **2** 492

[108] Evlyukhin A B *et al* 2014 Optical spectroscopy of single Si nanocylinders with magnetic and electric resonances *Sci. Rep.* **4** 4126

[109] Coenen T, van de Groep J and Polman A 2013 Resonant modes of single silicon nanocavities excited by electron irradiation *ACS Nano* **7** 1689–98

[110] Brönstrup G *et al* 2010 Optical properties of individual silicon nanowires for photonic devices *ACS Nano* **4** 7113–22

[111] Kruk S and Kivshar Y 2017 Functional meta-optics and nanophotonics governed by mie resonances *ACS Photonics* **4** 2638–49

[112] Person S *et al* 2013 Demonstration of zero optical backscattering from single nanoparticles *Nano Lett.* **13** 1806–9

[113] Ginn J C *et al* 2012 Realizing optical magnetism from dielectric metamaterials *Phys. Rev. Lett.* **108** 097402

[114] Ma C *et al* 2017 Directional scattering in a germanium nanosphere in the visible light region *Adv. Opt. Mater.* **5** 1700761

[115] Kerker M, Wang D S and Giles C L 1983 Electromagnetic scattering by magnetic spheres *J. Opt. Soc. Am.* **73** 765–7

[116] Geffrin J M *et al* 2012 Magnetic and electric coherence in forward- and back-scattered electromagnetic waves by a single dielectric subwavelength sphere *Nat. Commun.* **3** 1171

[117] Fu Y H *et al* 2013 Directional visible light scattering by silicon nanoparticles *Nat. Commun.* **4** 1527

[118] Gómez-Medina R 2011 Electric and magnetic dipolar response of germanium nanospheres: interference effects, scattering anisotropy, and optical forces *J. Nanophotonics* **5** 053512

[119] Lee J Y, Miroshnichenko A E and Lee R-K 2018 Simultaneously nearly zero forward and nearly zero backward scattering objects *Opt. Express* **26** 30393–9

[120] Staude I *et al* 2013 Tailoring directional scattering through magnetic and electric resonances in subwavelength silicon nanodisks *ACS Nano* **7** 7824–32

[121] Terekhov P D *et al* 2017 Resonant forward scattering of light by high-refractive-index dielectric nanoparticles with toroidal dipole contribution *Opt. Lett.* **42** 835–8

[122] Isro S D *et al* 2018 Engineering scattering patterns with asymmetric dielectric nanorods *Opt. Express* **26** 32624–30

[123] Krasnok A E *et al* 2015 Enhanced emission extraction and selective excitation of NV centers with all-dielectric nanoantennas *Laser Photonics Rev.* **9** 385–91

[124] Zalogina A S *et al* 2018 Purcell effect in active diamond nanoantennas *Nanoscale* **10** 8721–7

[125] Bakker R M *et al* 2015 Magnetic and electric hotspots with silicon nanodimers *Nano Lett.* **15** 2137–42

[126] Miri M and Sadrara M 2017 Dimers and trimers of hollow silicon nanoparticles: manipulating the magnetic hotspots *J. Phys. Chem.* C **121** 11672–9

[127] McPolin C P T *et al* 2018 Imaging electric and magnetic modes and their hybridization in single and dimer AlGaAs nanoantennas *Adv. Opt. Mater.* **6** 1800664

[128] Yao K and Liu Y 2018 Enhancing circular dichroism by chiral hotspots in silicon nanocube dimers *Nanoscale* **10** 8779–86

[129] Mohammadi E *et al* 2019 Accessible superchiral near-fields driven by tailored electric and magnetic resonances in all-dielectric nanostructures *ACS Photonics* **6** 1939–46

[130] Reyes Gómez F *et al* 2020 Enhanced chiroptical activity with slotted high refractive index dielectric nanodisks *Phys. Rev.* B **101** 155403

[131] Cambiasso J *et al* 2017 Bridging the gap between dielectric nanophotonics and the visible regime with effectively

lossless gallium phosphide antennas *Nano Lett.* **17** 1219–25

[132] Xu Z, Song W and Crozier K B 2018 Optical trapping of nanoparticles using all-silicon nanoantennas *ACS Photonics* **5** 4993–5001

[133] Sortino L *et al* 2019 Enhanced light–matter interaction in an atomically thin semiconductor coupled with dielectric nano-antennas *Nat. Commun.* **10** 5119

[134] Krasnok A *et al* 2016 Demonstration of the enhanced Purcell factor in all-dielectric structures *Appl. Phys. Lett.* **108** 211105

[135] Sugimoto H and Fujii M 2017 Colloidal dispersion of subquarter micrometer silicon spheres for low-loss antenna in visible regime *Adv. Opt. Mater.* **5** 1700332

[136] Mignuzzi S *et al* 2019 Nanoscale design of the local density of optical states *Nano Lett.* **19** 1613–7

[137] Pellegrini G, Mattei G and Mazzoldi P 2009 Light extraction with dielectric nanoantenna arrays *ACS Nano* **3** 2715–21

[138] Luk'yanchuk B *et al* 2010 The Fano resonance in plasmonic nanostructures and metamaterials *Nat. Mater.* **9** 707–15

[139] Huang Y *et al* 2019 Active tuning of the Fano resonance from a Si nanosphere dimer by the substrate effect *Nanoscale Horiz.* **4** 148–57

[140] Yang Z-J, Zhao Q and He J 2019 Fano interferences of electromagnetic modes in dielectric nanoblock dimers *J. Appl. Phys.* **125** 063103

[141] Gorodetsky M L, Savchenkov A A and Ilchenko V S 1996 Ultimate Q of optical microsphere resonators *Opt. Lett.* **21** 453–5

[142] Heylman K D *et al* 2017 Optical microresonators for sensing and transduction: a materials perspective *Adv. Mater.* **29** 1700037

[143] Foreman M R, Swaim J D and Vollmer F 2015 Whispering gallery mode sensors *Adv. Opt. Photonics* **7** 168–240

[144] Saleh B E and Teich M C 2019 *Fundamentals of Photonics* (New York: Wiley)

[145] Zhang Y and Lončar M 2009 Submicrometer diameter micropillar cavities with high quality factor and ultrasmall mode volume *Opt. Lett.* **34** 902–4

[146] Deotare P B *et al* 2009 High quality factor photonic crystal nanobeam cavities *Appl. Phys. Lett.* **94** 121106

[147] Safavi-Naeini A H *et al* 2010 Optomechanics in an ultrahigh-Q two-dimensional photonic crystal cavity *Appl. Phys. Lett.* **97** 181106

[148] Devilez A, Stout B and Bonod N 2010 Compact metallo-dielectric optical antenna for ultra directional and enhanced radiative emission *ACS Nano* **4** 3390–6

[149] Tiwari S *et al* 2020 Dielectric microsphere coupled to a plasmonic nanowire: a self-assembled hybrid optical antenna *Adv. Opt. Mater.* **8** 1901672

[150] Vasista A B, Tiwari S and Kumar G V P 2019 Wavevector distribution of metal photoluminescence from a gold film coupled microsphere antenna *J. Opt.* **21** 035002

[151] Gao Y and Shi Y 2019 Design of a single nanoparticle trapping device based on bow-tie-shaped photonic crystal nanobeam cavities *IEEE Photonics J.* **11** 4500408

[152] Xu Z and Crozier K B 2019 All-dielectric nanotweezers for trapping and observation of a single quantum dot *Opt. Express* **27** 4034–45

[153] Yu Y *et al* 2012 Dielectric core–shell optical antennas for strong solar absorption enhancement *Nano Lett.* **12** 3674–81

[154] Grinblat G *et al* 2016 Enhanced third harmonic generation in single germanium nanodisks excited at the anapole mode *Nano Lett.* **16** 4635–40

[155] Camacho-Morales R *et al* 2016 Nonlinear generation of vector beams from AlGaAs nanoantennas *Nano Lett.* **16** 7191–7

[156] Smirnova D A *et al* 2016 Multipolar third-harmonic generation driven by optically induced magnetic resonances *ACS Photonics* **3** 1468–76

[157] Carletti L *et al* 2015 Enhanced second-harmonic generation from magnetic resonance in AlGaAs nanoantennas *Opt. Express* **23** 26544–50

[158] Shcherbakov M R *et al* 2014 Enhanced third-harmonic generation in silicon nanoparticles driven by magnetic response *Nano Lett.* **14** 6488–92

[159] Golla C, Weber N and Meier C 2019 Zinc oxide based dielectric nanoantennas for efficient nonlinear frequency conversion *J. Appl. Phys.* **125** 073103

[160] Gili V F *et al* 2016 Monolithic AlGaAs second-harmonic nanoantennas *Opt. Express* **24** 15965–71

[161] Sauvan C *et al* 2013 Theory of the spontaneous optical emission of nanosize photonic and plasmon resonators *Phys. Rev. Lett.* **110** 237401

[162] Bogdanov S *et al* 2017 Electron spin contrast of Purcell-enhanced nitrogen-vacancy ensembles in nanodiamonds *Phys. Rev.* B **96** 035146

[163] Grier D G 2003 A revolution in optical manipulation *Nature* **424** 810–6

[164] Spesyvtseva S E S and Dholakia K 2016 Trapping in a material world *ACS Photonics* **3** 719–36

[165] Krasnok A *et al* 2018 Spectroscopy and biosensing with optically resonant dielectric nanostructures *Adv. Opt. Mater.* **6** 1701094

[166] Mannino G *et al* 2015 Octahedral faceted Si nanoparticles as optical traps with enormous yield amplification *Sci. Rep.* **5** 8354

[167] Dmitriev P A *et al* 2016 Resonant Raman scattering from silicon nanoparticles enhanced by magnetic response *Nanoscale* **8** 9721–6

[168] Rose A, Huang D and Smith D R 2013 Nonlinear interference and unidirectional wave mixing in metamaterials *Phys. Rev. Lett.* **110** 063901

[169] Shibanuma T *et al* 2017 Efficient third harmonic generation from metal–dielectric hybrid nanoantennas *Nano Lett.* **17** 2647–51

[170] Hao S, Chen G and Yang C 2013 Sensing using rare-earth-doped upconversion nanoparticles *Theranostics* **3** 331–45

[171] Cai X *et al* 2017 Reduction of pulmonary toxicity of metal oxide nanoparticles by phosphonate-based surface passivation *Part. Fibre Toxicol.* **14** 13

[172] Simovski C R *et al* 2013 Photovoltaic absorption enhancement in thin-film solar cells by non-resonant beam collimation by submicron dielectric particles *J. Appl. Phys.* **114** 103104

[173] Yao Y *et al* 2012 Broadband light management using low-Q whispering gallery modes in spherical nanoshells *Nat. Commun.* **3** 664

[174] Kim S-K *et al* 2014 Doubling absorption in nanowire solar cells with dielectric shell optical antennas *Nano Lett.* **15** 753–8

[175] Fan Z *et al* 2010 Ordered arrays of dual-diameter nanopillars for maximized optical absorption *Nano Lett.* **10** 3823–7

[176] https://refractiveindex.info/

[177] Sarkar S *et al* 2019 Hybridized guided-mode resonances via colloidal plasmonic self-assembled grating *ACS Appl. Mater. Interfaces* **11** 13752–60

[178] Gao L, Lemarchand F and Lequime M 2012 Exploitation of multiple incidences spectrometric measurements for thin film reverse engineering *Opt. Express* **20** 15734–51

[179] Kischkat J *et al* 2012 Mid-infrared optical properties of thin films of aluminum oxide, titanium dioxide, silicon dioxide, aluminum nitride, and silicon nitride *Appl. Opt.* **51** 6789–98

[180] Green M A and Keevers M J 1995 Optical properties of intrinsic silicon at 300 K *Prog. Photovoltaics Res. Appl.* **3** 189–92

[181] Li H H 1980 Refractive index of silicon and germanium and its wavelength and temperature derivatives *J. Phys. Chem. Ref. Data* **9** 561–658

[182] Larruquert J I *et al* 2011 Self-consistent optical constants of SiC thin films *J. Opt. Soc. Am.* A **28** 2340–45

[183] Aspnes D E *et al* 1986 Optical properties of $Al_xGa_{1-x}As$ *J. Appl. Phys.* **60** 754–67

[184] Adachi S 1989 Optical dispersion relations for GaP, GaAs, GaSb, InP, InAs, InSb, $Al_xGa_{1-x}As$, and $In_{1-x}Ga_xAsyP_{1-y}$ *J. Appl. Phys.* **66** 6030–40

[185] Amotchkina T *et al* 2020 Characterization of e-beam evaporated Ge, YbF3, ZnS, and LaF3 thin films for laser-oriented coatings *Appl. Opt.* **59** A40–A47

[186] Ciesielski A *et al* 2018 Permittivity of Ge, Te and Se thin films in the 200–1500 nm spectral range. Predicting the segregation effects in silver *Mater. Sci. Semicond. Process.* **81** 64–7

[187] Staude I and Schilling J 2017 Metamaterial-inspired silicon nanophotonics *Nat. Photonics* **11** 274–84

[188] Sarangan A 2016 Nanofabrication *Fundamentals and Applications of Nanophotonics* (Woodhead Publishing) ch 5 149–84

[189] Shankar K S and Raychaudhuri A K 2005 Fabrication of nanowires of multicomponent oxides: review of recent advances *Materials Science and Engineering:* C **25** 738–51

[190] Kalantar-zadeh K and Fry B 2008 Nano fabrication and patterning techniques *Nanotechnology-Enabled Sensors* (Boston, MA: Springer US) pp 135–210

[191] Lim A E-J *et al* 2014 Review of silicon photonics foundry efforts *IEEE J. Sel. Top. Quantum Electron.* **20** 405–16

[192] Thomson D *et al* 2016 Roadmap on silicon photonics *J. Opt.* **18** 073003

[193] Bogaerts W and Chrostowski L 2018 Silicon photonics circuit design: methods, tools and challenges *Laser Photonics Rev.* **12** 1700237

[194] Muñoz P *et al* 2017 Silicon nitride photonic integration platforms for visible, near-infrared and mid-infrared applications *Sensors* **17** 2088

[195] Elshaari A W *et al* 2020 Hybrid integrated quantum photonic circuits *Nat. Photonics* **14** 285–98

[196] He J *et al* 2020 Nonlinear nanophotonic devices in the ultraviolet to visible wavelength range *Nanophotonics* **9** 3781–804